Signal Processing and Computing

Master's Thesis

Implementation, Performance Assessment, and Refinement of Selected Distributed Localization Algorithms for Cooperative Wireless Networks

June 6, 2013

Michael Bak Koldsgaard

School of Information and Communication Technology

Aalborg University

AALBORG UNIVERSITY
STUDENT REPORT

School of Information and Communication Technology
Selma Lagerlöfsvej 300
9220 Aalborg Ø
http://sict.aau.dk

Title:
Implementation, Performance Assessment, and Refinement of Selected Distributed Localization Algorithms for Cooperative Wireless Networks

Project period:
September 2012 to June 2013

Group name:
13gr1074

Group members:
Michael Bak Koldsgaard

Supervisors:
Bernard Henri Fleury
Burak Cakmak

Copies: 4

Pages: 50

Enclosure: CD-ROM

Completed: June 6, 2013

Danish Summary

Denne opgave omhandler algoritmer til lokalisering af mobile enheder i et trådløse netværk. Mere specifikt lokalisering til indendørsbrug hvor fx GPS-signaler ikke er tilgængelige eller utilregnelige. Opgaven giver læseren en hurtig introduktion til lokaliseringsteknikker og de problemer der er forbundet med at udføre lokalisering i indendørs omgivelser. Dette indbefatter bl.a. problemer med forhindringer som møbler og vægge, der gør det problematisk at opnå gode estimater for den direkte afstand mellem to enheder.

Ved traditionel lokalisering anvender mobile enheder kun målinger fra fastplaceret punkter, som fx basestationer. Men ved at lade mobile enheder samarbejde om lokaliseringopgaven kan der opstå en synergieffekt hvor to mobile enheders tvetydige lokaliseringsestimater kan reduceres til et enkelt korrekt estimat.

Opgaven tager udgangspunkt i en lokaliseringsalgoritme baseret på såkaldt "Variational Message Passing". Dette er en methode til at approximere en kompleks pdf med en simplere pdf med minimal informationsforskel.

I dette projekt bliver den oprindelige algoritme udvidet til at inkludere et bimodal estimat i forhold til det oprindelige unimodal estimat. Begge algoritmer er blevet implementeret og testet, og den opgave fremviser nogle af resultater.

Det bliver via Monte Carlo simuleringer påvist at den foreslåede udvidelse kan give forbedrede postionsestimater. Dette kommer dog på bekostning af forøget beregningskompleksitet. Foruden simulerede data så testes algoritmerne også på data fra fysiske målinger foretaget via det EU-finansierede WHERE2-projekt, som denne opgave er en del af.

Preface

This Master's thesis presents the findings from my Master's project at the Signal Processing and Computing programme from the School of Information and Communication Technology at Aalborg University. The project has been carried out in the period from September 2012 to June 2013.

The objective of this project has been to implement the Variational Message Passing (VMP) algorithm for indoor localization by Pedersen et al. [1] with the goal of performance assessment and further refinement. The introductory parts of this thesis should give the reader the requisite background knowledge of indoor localization to asses the results.

This work has been performed within the framework of the WHERE2 (ICT-248894) project, which is partly funded by the European Commission.

References are cited using IEEE style, i.e. a citation number in square brackets. The references are listed on page 50. The enclosed CD-ROM contains the thesis as a PDF file, MATLAB code for the figures and algorithm implementation, and the experimental data. For convenience the content of the CD-ROM is also available online at `http://vmp.koldsgaard.dk`. File references are presented as ▶`/folder/filename.ext`. When the thesis is viewed as a PDF these references function as links to the online version of the files.

Thanks to my supervisors Bernard Henri Fleury and Burak Cakmak for their guidance and inputs. My collaboration with Burak on the some of the topics have been very rewarding and helpful. I would also like to thank Gerhard Steinböck for the many hours he spent helping me analyzing raw measurement data and navigating within the WHERE2 project.

Aalborg University, June 6, 2013

Michael Bak Koldsgaard

Contents

1 Introduction

This Master's project started with a project proposal stated as: implement, assess performance, and refine the Variational Message Passing algorithm for indoor localization by Pedersen et al. [1]. The project has included many types of different tasks like familiarization with the fields of indoor localization and variational message passing in general, implementing a preliminary version of the algorithm, testing the algorithm on simulated scenarios and on real measurements, evaluating the experience from these tests, proposing improvements of the algorithm, implementing new versions of the algorithm including improvements, and more. This thesis will describe some of the most important things learned from the this work including considerations, experiences, and actual results from within the field of indoor localization.

The main result of this work is a bimodal extension of the algorithm. Simulations show that this extension improves the average localization error compared to the original unimodal version of the algorithm. However the performance improvement comes at the expense of added computational load, and the performance improvement is only prominent in some scenarios. This leaves the bimodal extension as a trade off between performance and computational load. To make a fair valuation of this added computational load it is necessary to further asses efficient implementation schemes.

This project has been a part of the WHERE2 project. The WHERE2 project is an EU funded project with a threefold objective of developing indoor localization techniques, utilizing this location information for improving wireless communication, and realizing all of this in hardware to confirm the improvements with real measurement data [2].

The thesis is structured in 6 chapters. The remaining part of this chapter (Section 1.1) gives an introduction to the concepts of indoor localization and the challenges at hand. This section furthermore introduces the terminology from indoor localization that will be used throughout the thesis. Chapter 2 describes the theory and concepts behind the Variational Message Passing algorithm and elaborate on some of the details. Chapter 3 introduces the bimodal extension of the algorithm. Chapter 4 describes how the algorithms was implemented. Chapter 5 present results from some of the conducted simulations and results from real world data from the WHERE2 project. Chapter 6 wraps up the thesis with a conclusion of the achieved results.

1.1 Indoor localization

The concept of indoor localization is the equivalent of the well-known GPS positioning for outdoor scenarios. Although consumer-grade GPS receiver accuracy have improved over the years indoor environments and dense high-rise urban scenarios are still a challenge. GPS signals might not be available or unreliable, which might result in position accuracies that are impractical for many applications [3]. For indoor localization to be useful for a wide range of applications it should have a fairly good accuracy that is at least accurate to the right room on the right floor and hopefully much better than that.

Many types of applications could benefit or spawn from accurate indoor localization, e.g. indoor turn-by-turn navigation, emergency service assistance, security, location-based

notifications, games, information of nearest coffee maker or toilet, tracking of goods, or tracking of people that are late for meetings. For wireless communication accurate position estimates could be used to optimize the resource utilization, and as mentioned this is one of the main objectives of the WHERE2 project. The type of devices to be located range from small wireless sensors to smartphones to larger objects like indoor vehicles. In this work a specific application is not selected and generic terms are used to refer to the devices. All devices are termed "nodes" and these are divided into the two groups "anchor nodes" and "mobile nodes". Anchor nodes are nodes with a known position, e.g. a WiFi access point at a known position. Mobile nodes are nodes with an unknown position, e.g. a smartphone carried around by the user. The mobile nodes are the ones to be located. Mobile nodes need not necessarily be moving and could be stationary at an unknown position, e.g. a laptop on an office desk. Furthermore anchor nodes need not necessarily be at a fixed position and need not be part of a communication network as such. It could simply be a "dumb" device that broadcast beacons solely for localization purposes. The important thing is that its position is known at all times, e.g. like the GPS satellites whose positions are always predictable even though they orbit the Earth in a non-geosynchronous manner.

1.1.1 Measurements

To perform localization some measurements needs to be gathered that the position estimation can be be based on. Two popular measures are range and angle estimation. In range estimation the distance between two nodes is measured. These range measurements can then be used to indicate possible positions in the form of circles in the 2D case (spheres for 3D). This is illustrated in Figure 1.1(a). The the common intersection of these circles can then be used as a position estimate of the mobile node. This method is known as trilateration. For angle estimation nodes determines from which direction the incoming signals arrive. These measured angles of arrival can then be used to present a line on which the transmitting node most be located. The intersection of these lines gives an estimate of the position of the mobile node (see Figure 1.1(b)). This is known as triangulation.

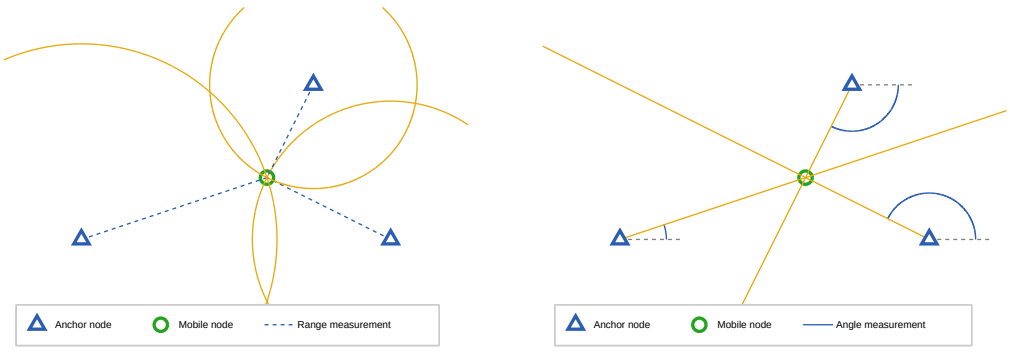

(a) (b)

Figure 1.1: Two types of measurements that can be used for position estimation. (a) Range measurements. (b) Angle measurements.

Angle measurements is sometimes referred to as AOA (Angle of Arrival). To perform angle estimation some form of antenna array is needed. The orientation of a node should

be consistent throughout an angle measurement or compensated for. Hand-held devices might experience problems with signal obstruction by the users hand for some angles of arrival. Localization based solely on angle estimates might be somewhat problematic since reliable knowledge of the device orientation is needed.

Range estimations can be done in two ways; measuring transmission delay or signal strength. Radio waves propagate according to the inverse-square law and hence the received signal strength decays with the distance. So by measuring the received signal strength the distance can be inferred. Measures of signal strength is often referred to as RSS (Received Signal Strength) or RSSI (Received Signal Strength Indicator). The main problem with RSS is that walls and other obstructions reduce the received signal strength [4], and hence such measurements would seem like being transmitted from further away than what was actually the case. Furthermore reliable measurements require some calibration of the sender and receiver, at least such that the receiver knows the transmitted signal power. Using some measure of transmission delay is an another form of range estimation. With the transmission delay and propagation rate of radio waves the distance can be calculated. Determining the transmission delay can be done in multiple ways. One method is to have some form accurate time synchronization, and then calculating the difference between the timestamps of transmit and receive. This is known as TOA (Time of Arrival). Another way is to use some form of round-trip method, i.e. where the receiver returns a message upon arrival of the a message from the transmitter. The total round-trip time divided by two can then be used as measure of the transmission delay. Round-trip systems should compensate for the time delay introduced by the receiver not responding instantly. This is known as RTD (Round-Trip Delay time).

Another type of localization technique is multilateration. Here TDOA (Time Difference of Arrival) is measured between two or more spatially separated nodes. With multiple such synchronized receiver nodes at known positions it is possible to locate the transmitting node. TDOA is also used to describe the measurements within a node that performs angle of arrival estimation with an antenna array.

1.1.2 Challenges of indoor measurements

Performing useful and reliable measurements in indoor environments is however not trivial. Non-line-of-sight (NLOS) conditions often arise in indoor environments due to walls and furniture. This can lead to decreased signal strength (problematic for RSS measurements), but it can also be the root of a much tougher problem: signals not taking the direct route. Radio waves propagate in all direction (assuming an isotropic antenna) and while radio waves do penetrate most walls they also reflect of surfaces. This leads to multiple paths of signal propagation from device A to device B. This is know as multipath propagation. This is a serve challenge for indoor localization as the measured signal might not contain the direct line-of-sight (LOS) component. For range estimation this would result in longer estimates than would have been the case for line-of-sight-only measurements. For angle estimation this is even a larger problem as the strongest component might appear from a different angle than the direction of the transmitting node.

Another problem of indoor localization is the possible low number of anchor nodes within communication range. For unambiguous localization in 3 dimensions using tri-

lateration a minimum of 4 anchors is needed. However the number of anchors within reliable communication range in an indoor scenario might not always be 4. And even if 4 anchors are available they may provide unreliable range estimations due to multipath propagation. Installing at least 4 anchor nodes in each room would of course reduce this problem (assuming empty and convex shaped rooms), but it would likely be impractical or too costly.

1.1.3 Cooperation

To overcome the difficulties of a low number of reliable anchor nodes it might be beneficial to let the mobile nodes cooperate for localization. Figure 1.2 shows how two mobile nodes can benefit from cooperation. Mobile node m_1 is connected to anchor node a_1 and a_3, and mobile node m_2 is connected to anchor node a_2 and a_3. Assuming range based 2-dimensional localization both mobile node m_1 and m_2 can not unambiguously determine their positions. Mobile node m_1 could be located in either intersection i_1 or i_2 whereas mobile node m_2 could be in i_3 or i_4. However if the two mobile nodes cooperate and measure the distance between them this distance could be used to determine that the only possible configuration is that m_1 is in i_1 and m_2 in i_3. This is main idea of cooperative localization. Cooperative localization requires communication between the mobile nodes to enable them to help each other. In the example of Figure 1.2 that could be mobile node m_1 sending its possible position coordinates of i_1 and i_2 to mobile node m_2, that would then be able to determine its position unambiguously using the inter-distance of the two mobile nodes. The position of m_2 should then be returned to m_1 enabling it to as well determine its position.

The concept of cooperative localization shown in Figure 1.2 can of course be used in even more complex scenarios where some mobile nodes might only have connections to other mobile nodes and not to any anchor nodes.

1.1.4 Distributed vs. centralized

One of the main considerations for a localization scheme is where the computation of the position estimates should occur. For non-cooperative localization, like GPS positioning, the computation is often carried out by the mobile node itself. However this computation could be done centralized by the anchor nodes or another compute device on the network. For cooperative localization the idea of centralized localization is even more attractive as the needed communication between the mobile nodes could be eliminated. In the example from Figure 1.2 that would mean that all range measurements from the mobile nodes including the measured inter-distance would be sent to a central compute unit on the network that would then return the estimated positions to the two mobile nodes. The most suitable scheme depends on the application at hand. However determining which one is the most suitable is not trivial. Constraints on privacy, energy consumption, mobile node computational power, required position estimation update interval, and network communication limitations are just some of the things to consider. E.g. for a network of mobile low-powered low-cost wireless sensors it is probably most desirable to do the localization computation on the device that handles all the sensor readings away such that the position estimates are synchronized with the sensor readings. Another example could

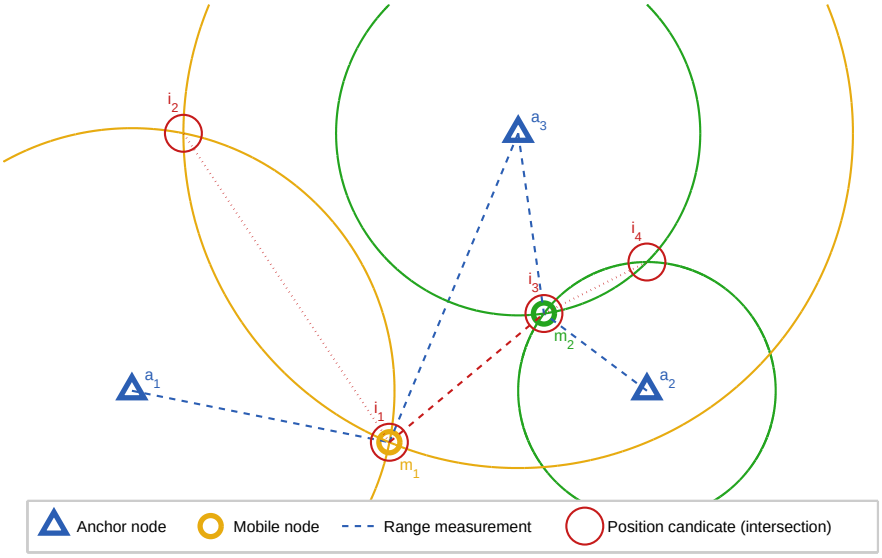

Figure 1.2: With cooperative localization ambiguities can be solved. Without cooperation mobile node m_1 would not know whether it was located in intersection i_1 or i_2, and mobile node m_2 in i_3 or i_4. However by measuring their inter-distance (red dashed line) the mobile nodes can both unambiguously determine their correct positions.

be an office network of powerful smartphones and laptops. These mobile nodes could perform the computations themselves and exchange information with their neighbouring nodes in the process.

1.1.5 Algorithm categories

Localization algorithms generally fall into two categories; geometric and statistical [5]. Geometric algorithms use the measurements as is (assuming LOS conditions) to compute the best position estimate in some sense, e.g. a least squares error measure. Statistical based algorithms assign some uncertainty to the measurements and perform statistical inference using general purpose statistical methods. These uncertainties could be assigned in multiple ways, but should of course aim to describe the underlying distributions as truthfully as possible. This is however not a trivial task since the measurement error might be caused by multipath NLOS conditions rather that measurement noise.

An alternative way to do localization that does not fall into the two other categories is fingerprinting [3]. Fingerprinting is a mapping scheme where range measurements (RSS and/or TOA) from each anchor node are collected and stored for each position of interest. These points of interest could be arranged as a grid of points in a room. A set of measurements for a specific point is called a fingerprint. To do localization the same measurements are performed by a mobile node and these results are then looked up in the database of fingerprints where the best match is then used as the position estimate. However the fingerprinting scheme has some drawbacks. One is that the fingerprints needs to be collected and this might include some costly manual work. Another drawback is that two fingerprints from different locations might be similar and indistinguishable by a mobile node.

New algorithms that are specifically tailored for indoor localization have appeared

recently. These algorithms exploit that UWB (Ultra WideBand) signals might contain information on the mutlipath components and that these components along with detailed floor plan information can be used for localization with only one anchor node [6]. In these algorithms the NLOS multipath components are used as range measurements from virtual anchors. A virtual anchor represent the location from which a signal would appear to be coming from if the signal from the physical anchor is reflected of a wall or other surface. These techniques have been combined with cooperation in [7] and [8]. While these algorithms are certainly interesting this extra information of multipath components within UWB signals have not been included in this project.

2 Variational Message Passing (VMP)

The Variational Message Passing (VMP) algorithm for indoor localization by Pedersen et al. [1] has been the main focus of this project and this section will give an introduction to the algorithm. The algorithm can by classified as one of the statistical types of algorithms for localization. The algorithm has a simplistic approach to localization by considering a network of nodes as a probabilistic graphical model where the node pairs are connected if they have performed a range measurement between them. This gives the simple interpretation that nodes in the graph corresponds to physical nodes, and that the localization problem can be solved by inference on the graph. The algorithm consider only range measurements and the estimated uncertainty of these. Hence it does not care how these measurements are obtained be it RSS, TOA, RTD, or something else.

Using a slightly modified version of the notation from [1] the graph can be defined as a set of nodes $\mathcal{N}$ and a set of edges $\mathcal{E}$. Each physical node with index r is defined as a node $r \in \mathcal{N}$ in the graph, and edges $(r,t) \in \mathcal{E}$ in the graph represents the link between nodes r and t where a range measurement has been performed. An example of such a graph can be seen in [1, Fig. 1]. The subsets of mobile and anchor nodes are represented by $\mathcal{N}_M$ and $\mathcal{N}_A$, respectively.

The true position of a node is represented by a vector $\boldsymbol{\mu}_r \in \mathbb{R}^2$. Note that like in [1] this thesis will only consider localization in 2 dimensions, but an extension to 3 dimensions is straightforward. Any prior knowledge of the position of a mobile node is represented by a circular symmetric Gaussian with mean $\tilde{\boldsymbol{\mu}}_m$ and variance $\tilde{\sigma}_m^2$. The distance measures between two nodes is represented by:

$$d_{r,t} = ||\boldsymbol{\mu}_r - \boldsymbol{\mu}_t|| + w_{r,t} \tag{2.1}$$

where $||\cdot||$ is the Euclidean norm and $w_{r,t}$ is the independent observation noise. In [1] this observation noise is defined as a zero-mean Gaussian with variance $\sigma^2_{d_{r,t}}$. This choice is an important one since it simplifies the algorithm, but at the same time it is questionable whether this distribution describes all the types of range measurements fed into the algorithm.

Now defining a set of all node position vectors as $\mathcal{X} = \{\boldsymbol{x}_r : r \in \mathcal{N}\}$ and a set of all distance measurements as $\mathcal{D} = \{d_{r,t} : (r,t) \in \mathcal{E}\}$ the joint pdf for a localization scenario can be described as (like [1, eq. 2 and 3]):

$$p(\mathcal{X}, \mathcal{D}) = p(\mathcal{D}|\mathcal{X})\, p(\mathcal{X}) \tag{2.2}$$

$$= \left(\prod_{(r,t)\,\in\,\mathcal{E}} \mathcal{N}\left(d_{r,t} \mid ||\boldsymbol{x}_r - \boldsymbol{x}_t||, \sigma^2_{d_{r,t}}\right) \right) \left(\prod_{m\,\in\,\mathcal{N}_M} \mathcal{N}\left(\boldsymbol{x}_m \mid \tilde{\boldsymbol{\mu}}_m, \tilde{\sigma}^2_m\right) \right) \tag{2.3}$$

where for notational convenience $\mathcal{N}(\cdot \mid \cdot, \sigma^2)$ is used for both the one-dimensional Gaussian pdf and the circular symmetric 2-dimensional pdf $\mathcal{N}(\cdot \mid \cdot, \sigma^2\mathbf{I})$. This joint pdf can be

represented as a factor graph with the variable nodes $\mathcal{X}$ and the following factors:

$$f_m(\boldsymbol{x_m}) = \mathcal{N}\left(\boldsymbol{x}_m \,|\, \tilde{\boldsymbol{\mu}}_m, \tilde{\sigma}_m^2\right) \tag{2.4}$$

$$g_{r,t}(\boldsymbol{x}_r, \boldsymbol{x}_t) = \mathcal{N}\left(d_{r,t} \,|\, ||\boldsymbol{x}_r - \boldsymbol{x}_t||, \sigma_{d_{r,t}}^2\right) \tag{2.5}$$

Note that the value of variable nodes $\mathcal{X}_A = \{\boldsymbol{x}_a : a \in \mathcal{N}_A\}$ will be considered as observed variables since these are the known positions of the anchor nodes. An example of such a factor graph is shown in Figure 2.1, where the factor nodes names are shown in short form like f_m and $g_{r,t}$.

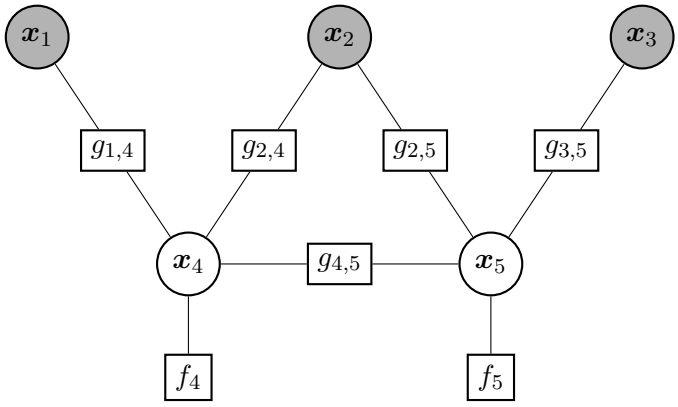

Figure 2.1: Example of factor graph representing a scenario similar to the one shown in Figure 1.2. Gray variable nodes represent observed variables (anchor node positions).

Having expressed the localization problem in the form of a factor graph makes it easier to apply graphical inference methods. Note that like in the example of Figure 2.1 the graphs will generally contain loops and hence exact inference might be intractable. Message passing algorithms can be used to solve such problems by approximating the complex Bayesian network with a simpler network with minimum information divergence [9]. The use of approximations implies that the solutions might be sub-optimal. Multiple such message passing algorithms exist, e.g. loopy belief propagation, expectation propagation, and variational message passing. According to [9] they differ by the measure of information divergence they try to minimize, e.g. inclusive vs. exclusive Kullback-Leibler divergence.

The variational message passing (VMP) algorithm is based on the mean field assumption and the exclusive Kullback-Leibler (KL) divergence. The mean field assumption refers to the assumption that the complex pdf $p(\mathcal{X}|\mathcal{D})$ can be approximated by a simpler pdf $q(\mathcal{X})$ that factorizes into $q(\mathcal{X}) = \prod_{\boldsymbol{x}_i \in \mathcal{X}} q_i(\boldsymbol{x}_i)$. The used divergence measure is the KL-divergence:

$$\mathrm{KL}\left(q(\mathcal{X}) \parallel p(\mathcal{X}|\mathcal{D})\right) = \int_{\mathcal{X}} q(\mathcal{X}) \ln \frac{q(\mathcal{X})}{p(\mathcal{X}|\mathcal{D})} \, d\mathcal{X} \tag{2.6}$$

Since the KL-divergence measure is not symmetric it is important to note that the used measure of VMP is $\mathrm{KL}\left(q \parallel p\right)$. This form is termed exclusive and zero-forcing by Minka [9] since it forces q to be small when p is small. On the other hand the form $\mathrm{KL}\left(p \parallel q\right)$ is termed inclusive as q would try to include more of p even if q would have to include areas where p is small. An example of this is shown in [9, Fig. 1]. The messages of the VMP

algorithm are defined as [1]:

$$m_{f_r \to \boldsymbol{x}_r}(\boldsymbol{x}_r) = f_r(\boldsymbol{x}_r) \tag{2.7}$$

$$m_{g_{r,t} \to \boldsymbol{x}_r}(\boldsymbol{x}_r) = \exp\left(\int_{\boldsymbol{x}_t} m_{\boldsymbol{x}_t \to g_{r,t}}(\boldsymbol{x}_t) \ln g_{r,t}(\boldsymbol{x}_r, \boldsymbol{x}_t)\, d\boldsymbol{x}_t \right) \tag{2.8}$$

$$m_{\boldsymbol{x}_r \to g_{r,t}}(\boldsymbol{x}_r) = \tilde{p}_r(\boldsymbol{x}_r) = \frac{1}{Z} m_{f_r \to \boldsymbol{x}_r}(\boldsymbol{x}_r) \prod_{t \in \mathcal{N}_r} m_{g_{r,t} \to \boldsymbol{x}_r}(\boldsymbol{x}_r) \tag{2.9}$$

where $\mathcal{N}_r$ is the set of neighbouring nodes of the variable $\boldsymbol{x}_r$ and Z is the normalization constant such that $\int_{\boldsymbol{x}_r} \tilde{p}_r(\boldsymbol{x}_r)\, d\boldsymbol{x}_t = 1$. The message of (2.9) can become arbitrary complex to represent and lead to intractable computations. To avoid this problem the messages are restricted to be in the family of circular symmetric Gaussians [1]. This is done by approximating the messages $\tilde{p}_r(\boldsymbol{x}_r)$ with $q'_r(\boldsymbol{x}_r)$ belonging to this family with the least KL-divergence:

$$m^G_{\boldsymbol{x}_r \to g_{r,t}}(\boldsymbol{x}_r) = \underset{q'_r(\boldsymbol{x}_r) \in \mathcal{G}}{\arg\min}\, \mathrm{KL}\left(q'_r(\boldsymbol{x}_r) \parallel \tilde{p}_r(\boldsymbol{x}_r) \right) \tag{2.10}$$

where $\mathcal{G}$ represents the family of circular symmetric Gaussians. The found $q'_r(\boldsymbol{x}_r)$ that minimizes the KL-divergence is fully represented by its mean $\hat{\boldsymbol{\mu}}_r$ and variance $\hat{\sigma}^2_r$.

In particle based belief propagation methods this problem of too complex messages is solved by representing the messages with a large number of particles, e.g. 200 particles per message in [10]. This would however result in a large communication overhead in a distributed localization scheme. For the VMP algorithm with the circular symmetric Gaussian restriction only the mean and variance needs to transmitted. In the case of 3-dimensional localization this would be 4 real values. This is the main advantage of VMP compared to particle based methods.

The VMP algorithm in all its simplicity is shown in Algorithm 1. Note that no stopping criterion is decided upon in [1]. For the simulations and study of the algorithm in this thesis the stopping criterion will simply be a fixed number of iterations. See chapter 4 for a discussion of the stopping criterion for a real world implementation.

Algorithm 1 The VMP algorithm [1].

Initialization:

for all nodes (in parallel) **do**
1) Obtain distance measurement to neighbouring nodes.
2) Broadcast distance measures and prior position knowledge to neighbouring nodes.
end for

Position estimation:

repeat
for all nodes (in parallel) **do**
1) Find $q'_r(\boldsymbol{x}_r)$ that minimizes $\mathrm{KL}\left(q'_r(\boldsymbol{x}_r) \parallel \tilde{p}_r(\boldsymbol{x}_r)\right)$.
2) Broadcast found parameters of $q'_r(\boldsymbol{x}_r)$ to neighbouring nodes.
3) Collect broadcasted messages from neighbouring nodes.
end for
until stopping criterion is reached.

2.1 Closed form expression for the KL-divergence

In (2.10) the message is constrained to a circular symmetric Gaussian with the least KL-divergence. However to find this $q'_r(\boldsymbol{x}_r)$ it is highly beneficial to have a closed form expression for the function to be minimized. Such an expression is not provided in [1] so it has been derived here. The expression for the KL-divergence to be minimized is stated as:

$$\mathrm{KL}\left(q'_r(\boldsymbol{x}_r) \parallel \tilde{p}_r(\boldsymbol{x}_r)\right) = \int_{\boldsymbol{x}_r} q'_r(\boldsymbol{x}_r) \ln \frac{q'_r(\boldsymbol{x}_r)}{\tilde{p}_r(\boldsymbol{x}_r)} \, d\boldsymbol{x}_r \tag{2.11}$$

where q'_r is a circular symmetric Gaussian with mean $\dot{\boldsymbol{\mu}}_r$ and variance $\dot{\sigma}_r^2$ (parameters for optimization) and $\tilde{p}_r$ defined as:

$$q'_r(\boldsymbol{x}_r) = \mathcal{N}(\boldsymbol{x}_r \,|\, \dot{\boldsymbol{\mu}}_r, \dot{\sigma}_r^2) \tag{2.12}$$

$$\tilde{p}_r(\boldsymbol{x}_r) = \frac{1}{Z} \, m_{f_r \to \boldsymbol{x}_r}(\boldsymbol{x}_r) \prod_{a \in \mathcal{N}_r \cap \mathcal{N}_A} m_{g_{r,a} \to \boldsymbol{x}_r}(\boldsymbol{x}_r) \prod_{m \in \mathcal{N}_r \cap \mathcal{N}_M} m_{g_{r,m} \to \boldsymbol{x}_r}(\boldsymbol{x}_r) \tag{2.13}$$

with Z being the normalization constant and:

$$m_{f_r \to \boldsymbol{x}_r}(\boldsymbol{x}_r) = \mathcal{N}(\boldsymbol{x}_r \,|\, \tilde{\boldsymbol{\mu}}_r, \tilde{\sigma}_r^2) \tag{2.14}$$

$$m_{g_{r,a} \to \boldsymbol{x}_r}(\boldsymbol{x}_r) = \mathcal{N}(d_{r,a} \,|\, ||\boldsymbol{x}_r - \boldsymbol{\mu}_a||, \sigma_{d_{r,a}}^2) \tag{2.15}$$

$$m_{g_{r,m} \to \boldsymbol{x}_r}(\boldsymbol{x}_r) = \exp\left(\int_{\boldsymbol{x}_m} q_m(\boldsymbol{x}_m) \ln \mathcal{N}(d_{r,m} \,|\, ||\boldsymbol{x}_r - \boldsymbol{x}_m||, \sigma_{d_{r,m}}^2) \, d\boldsymbol{x}_m\right) \tag{2.16}$$

$$= \exp\left(\mathbb{E}_{\boldsymbol{x}_m}\left[\ln \mathcal{N}(d_{r,m} \,|\, ||\boldsymbol{x}_r - \boldsymbol{x}_m||, \sigma_{d_{r,m}}^2)\right]\right) \tag{2.17}$$

Note that the messages from factor nodes $g_{r,t}$ are spilt into those from anchor nodes $g_{r,a}$ and from mobile nodes $g_{r,m}$. The messages from $g_{r,a}$ are simplified by considering $q_a(\boldsymbol{x}_a)$ of the observed variable as a Dirac delta function in $\boldsymbol{\mu}_a$. Now ignoring the normalization constant we can rewrite the KL-divergence as:

$$\mathrm{KL}\left(q'_r(\boldsymbol{x}_r) \parallel \tilde{p}_r(\boldsymbol{x}_r)\right) \propto \mathrm{KL}\left(q'_r(\boldsymbol{x}_r) \parallel \mathcal{N}(\boldsymbol{x}_r \,|\, \tilde{\boldsymbol{\mu}}_r, \tilde{\sigma}_r^2)\right) \tag{2.18a}$$

$$- \sum_{a \in \mathcal{N}_r \cap \mathcal{N}_A} \mathbb{E}_{\boldsymbol{x}_r}\left[\ln \mathcal{N}(d_{r,a} \,|\, ||\boldsymbol{x}_r - \boldsymbol{\mu}_a||, \sigma_{d_{r,a}}^2)\right] \tag{2.18b}$$

$$- \sum_{m \in \mathcal{N}_r \cap \mathcal{N}_M} \mathbb{E}_{\boldsymbol{x}_r}\left[\mathbb{E}_{\boldsymbol{x}_m}\left[\ln \mathcal{N}(d_{r,m} \,|\, ||\boldsymbol{x}_r - \boldsymbol{x}_m||, \sigma_{d_{r,m}}^2)\right]\right] \tag{2.18c}$$

For (2.18a) the closed form solution for a KL-divergence between two multivariate Gaussians can be used. In our case with a 2-dimensional circular symmetric Gaussians that is:

$$\mathrm{KL}\left(q'_r(\boldsymbol{x}_r) \parallel \mathcal{N}(\boldsymbol{x}_r \,|\, \tilde{\boldsymbol{\mu}}_r, \tilde{\sigma}_r^2)\right) = \frac{\dot{\sigma}_r^2}{\tilde{\sigma}_r^2} + \frac{||\dot{\boldsymbol{\mu}}_r - \tilde{\boldsymbol{\mu}}_r||^2}{2\tilde{\sigma}_r^2} - 1 - \ln \frac{\dot{\sigma}_r^2}{\tilde{\sigma}_r^2} \tag{2.19}$$

The contribution from each neighbouring anchor node can be written as:

$$\mathbb{E}_{\boldsymbol{x}_r}\left[\ln\mathcal{N}(d_{r,a}\mid||\boldsymbol{x}_r-\boldsymbol{\mu}_a||,\sigma^2_{d_{r,a}})\right]=\mathbb{E}_{\boldsymbol{x}_r}\left[\ln\frac{1}{\sqrt{2\pi\sigma^2_{d_{r,a}}}}-\frac{1}{2\sigma^2_{d_{r,a}}}(d_{r,a}-||\boldsymbol{x}_r-\boldsymbol{\mu}_a||)^2\right] \tag{2.20}$$

$$=\ln\frac{1}{\sqrt{2\pi\sigma^2_{d_{r,a}}}}-\frac{1}{2\sigma^2_{d_{r,a}}}\mathbb{E}_{\boldsymbol{x}_r}\left[(d_{r,a}-||\boldsymbol{x}_r-\boldsymbol{\mu}_a||)^2\right] \tag{2.21}$$

$$=\ln\frac{1}{\sqrt{2\pi\sigma^2_{d_{r,a}}}}-\frac{d^2_{r,a}-2d_{r,a}\mathbb{E}_{\boldsymbol{x}_r}\left[||\boldsymbol{x}_r-\boldsymbol{\mu}_a||\right]+\mathbb{E}_{\boldsymbol{x}_r}\left[||\boldsymbol{x}_r-\boldsymbol{\mu}_a||^2\right]}{2\sigma^2_{d_{r,a}}} \tag{2.22}$$

Using that $\boldsymbol{x}_r$ can be rewritten as $\dot{\boldsymbol{\mu}}_r+\bar{\boldsymbol{x}}_r$ with $\bar{\boldsymbol{x}}_r\sim\mathcal{N}(\boldsymbol{0},\dot{\sigma}^2_r)$:

$$\mathbb{E}_{\boldsymbol{x}_r}\left[||\boldsymbol{x}_r-\boldsymbol{\mu}_a||^2\right]=\mathbb{E}_{\bar{\boldsymbol{x}}_r}\left[||\bar{\boldsymbol{x}}_r+(\dot{\boldsymbol{\mu}}_r-\boldsymbol{\mu}_a)||^2\right] \tag{2.23}$$

$$=||\dot{\boldsymbol{\mu}}_r-\boldsymbol{\mu}_a||^2+\mathbb{E}_{\bar{\boldsymbol{x}}_r}\left[||\bar{\boldsymbol{x}}_r||^2\right]+2\,\mathbb{E}_{\bar{\boldsymbol{x}}_r}\left[\bar{\boldsymbol{x}}_r\right]^T(\dot{\boldsymbol{\mu}}_r-\boldsymbol{\mu}_a) \tag{2.24}$$

$$=||\dot{\boldsymbol{\mu}}_r-\boldsymbol{\mu}_a||^2+2\dot{\sigma}^2_r \tag{2.25}$$

Furthermore defining $R=||\bar{\boldsymbol{x}}_r+(\dot{\boldsymbol{\mu}}_r-\boldsymbol{\mu}_a)||$ we have that $R\sim\text{Rice}(||\dot{\boldsymbol{\mu}}_r-\boldsymbol{\mu}_a||,\sqrt{\dot{\sigma}^2_r})$ [11], hence:

$$\mathbb{E}_{\boldsymbol{x}_r}\left[||\boldsymbol{x}_r-\boldsymbol{\mu}_a||\right]=\mathbb{E}_{\bar{\boldsymbol{x}}_r}\left[||\bar{\boldsymbol{x}}_r+(\dot{\boldsymbol{\mu}}_r-\boldsymbol{\mu}_a)||\right] \tag{2.26}$$

$$=\mathbb{E}_R\left[R\right] \tag{2.27}$$

$$=\sqrt{\dot{\sigma}^2_r\tfrac{\pi}{2}}\,\mathrm{M}\left(-\frac{1}{2},1,-\frac{||\dot{\boldsymbol{\mu}}_r-\boldsymbol{\mu}_a||^2}{2\dot{\sigma}^2_r}\right) \tag{2.28}$$

where $\mathrm{M}(a,b,z)$ is the confluent hypergeometric function of the first kind [12]. Inserting (2.25) and (2.28) into (2.22) gives the contribution from each neighbouring anchor node:

$$\mathbb{E}_{\boldsymbol{x}_r}\left[\ln\mathcal{N}(d_{r,a}\mid||\boldsymbol{x}_r-\boldsymbol{\mu}_a||,\sigma^2_{d_{r,a}})\right]=$$
$$\ln\frac{1}{\sqrt{2\pi\sigma^2_{d_{r,a}}}}-\frac{d^2_{r,a}-2d_{r,a}\sqrt{\dot{\sigma}^2_r\tfrac{\pi}{2}}\,\mathrm{M}\left(-\frac{1}{2},1,-\frac{||\dot{\boldsymbol{\mu}}_r-\boldsymbol{\mu}_a||^2}{2\dot{\sigma}^2_r}\right)+||\dot{\boldsymbol{\mu}}_r-\boldsymbol{\mu}_a||^2+2\dot{\sigma}^2_r}{2\sigma^2_{d_{r,a}}} \tag{2.29}$$

Using a similar approach for the neighbouring mobile nodes with $\boldsymbol{x}_m=\hat{\boldsymbol{\mu}}_m+\bar{\boldsymbol{x}}_m$ and $\bar{\boldsymbol{x}}_{r+m}=\bar{\boldsymbol{x}}_r+\bar{\boldsymbol{x}}_m$ where $\bar{\boldsymbol{x}}_m\sim\mathcal{N}(\boldsymbol{0},\hat{\sigma}^2_m)$ and $\bar{\boldsymbol{x}}_{r+m}\sim\mathcal{N}(\boldsymbol{0},\dot{\sigma}^2_r+\hat{\sigma}^2_m)$ gives:

$$\mathbb{E}_{\boldsymbol{x}_r}\left[\mathbb{E}_{\boldsymbol{x}_m}\left[\ln\mathcal{N}(d_{r,m}\mid||\boldsymbol{x}_r-\boldsymbol{x}_m||,\sigma^2_{d_{r,m}})\right]\right]=\ln\frac{1}{\sqrt{2\pi\sigma^2_{d_{r,m}}}}$$
$$-\frac{d^2_{r,m}-2d_{r,m}\sqrt{(\dot{\sigma}^2_r+\hat{\sigma}^2_m)\tfrac{\pi}{2}}\,\mathrm{M}\left(-\frac{1}{2},1,-\frac{||\dot{\boldsymbol{\mu}}_r-\hat{\boldsymbol{\mu}}_m||^2}{2(\dot{\sigma}^2_r+\hat{\sigma}^2_m)}\right)+||\dot{\boldsymbol{\mu}}_r-\hat{\boldsymbol{\mu}}_m||^2+2(\dot{\sigma}^2_r+\hat{\sigma}^2_m)}{2\sigma^2_{d_{r,m}}} \tag{2.30}$$

Now using (2.19), (2.29), and (2.30) and ignoring all constant terms the KL-divergence can be written in closed form as:

$$\mathrm{KL}\left(q'_r \parallel \tilde{p}_r\right) \propto \frac{||\dot{\boldsymbol{\mu}}_r - \tilde{\boldsymbol{\mu}}_r||^2 + 2\dot{\sigma}_r^2}{2\tilde{\sigma}_r^2} - \ln \dot{\sigma}_r^2 \tag{2.31a}$$

$$+ \sum_{a \in \mathcal{N}_r \cap \mathcal{N}_A} \frac{-2d_{r,a}\sqrt{\dot{\sigma}_r^2 \frac{\pi}{2}}\,\mathrm{M}\left(-\frac{1}{2}, 1, -\frac{||\dot{\boldsymbol{\mu}}_r - \boldsymbol{\mu}_a||^2}{2\dot{\sigma}_r^2}\right) + ||\dot{\boldsymbol{\mu}}_r - \boldsymbol{\mu}_a||^2 + 2\dot{\sigma}_r^2}{2\sigma_{d_{r,a}}^2} \tag{2.31b}$$

$$+ \sum_{m \in \mathcal{N}_r \cap \mathcal{N}_M} \frac{-2d_{r,m}\sqrt{(\dot{\sigma}_r^2 + \hat{\sigma}_m^2)\frac{\pi}{2}}\,\mathrm{M}\left(-\frac{1}{2}, 1, -\frac{||\dot{\boldsymbol{\mu}}_r - \hat{\boldsymbol{\mu}}_m||^2}{2(\dot{\sigma}_r^2 + \hat{\sigma}_m^2)}\right) + ||\dot{\boldsymbol{\mu}}_r - \hat{\boldsymbol{\mu}}_m||^2 + 2\dot{\sigma}_r^2}{2\sigma_{d_{r,m}}^2} \tag{2.31c}$$

To do the numerical minimization a closed form expression for the gradient is found as well. This is shown in Appendix A. With this closed form expression for the KL-divergence the implementation of the VMP algorithm is straightforward.

3 Bimodal Variational Message Passing (B-VMP)

This chapter concerns the "refinement" part of the project. The algorithm from [1] described in chapter 2 was implemented for initial performance assessment purposes. From simulations similar to the ones described in [1, Sec. V] it was clear that scenarios where some of the mobile nodes failed to be located was the most interesting. A simple simulation scenario was constructed to investigate these problems further. The simple simulation scenario is described in Section 5.1.

It was observed that in these simulations the position estimate for one or more mobile nodes would sometimes alternate between two distinct positions for each iteration rather that improve one of them. Figure 3.1 illustrates such an example where the position estimation error is shown for each mobile node for each iteration. Note that this figure only consists of $10 \cdot 16$ discrete values, and that the contours in between these are just interpolations used to easier visualize the change from one iteration to another. In this example mobile node 1 and 9 both alternate between a good position estimate (blue) and a worse position estimate (red) for all iterations whereas the other nodes seem to have found more stable position estimates.

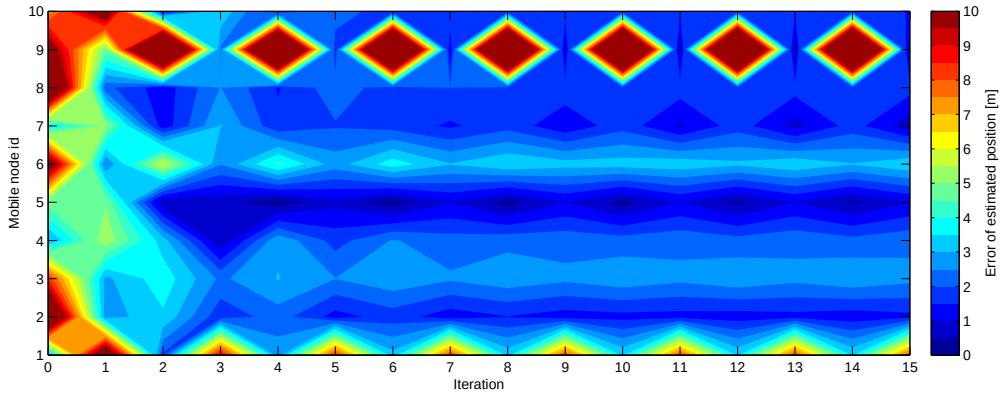

Figure 3.1: Example of convergence for the VMP algorithm. The figure shows the position estimate error for each mobile node for each iteration.

This behaviour is of course caused by the interaction of the mobile nodes via the messages of new beliefs. Since these changes of belief for one or more neighbouring nodes could cause a mobile node to continuously alternate between two position estimates it was clear that an inherent or arising ambiguity in the system was not fully modelled.

Looking at a simple 1-dimensional example of a belief based on erroneous measurements it is clear that the simple unimodal representation in [1] might not be sufficient. Figure 3.2 shows such an example. For simplicity just two erroneous anchor distance measurements are shown with their appertaining messages. Below the graph is an illustration of the distance measurements $d_{r,t}$ and their ± 1 standard deviation $\sigma_{d_{r,t}}$. It is clear that in such a case the product of the messages would be bimodal (green line). To underline the point of this example it is constructed such that the largest of the modes is the wrong

one, i.e. the true position of the mobile node (vertical dashed line) is closer to the smaller mode. A unimodal approximation with minimum KL $(q \parallel p)$ divergence from the product is shown as the red dashed line.

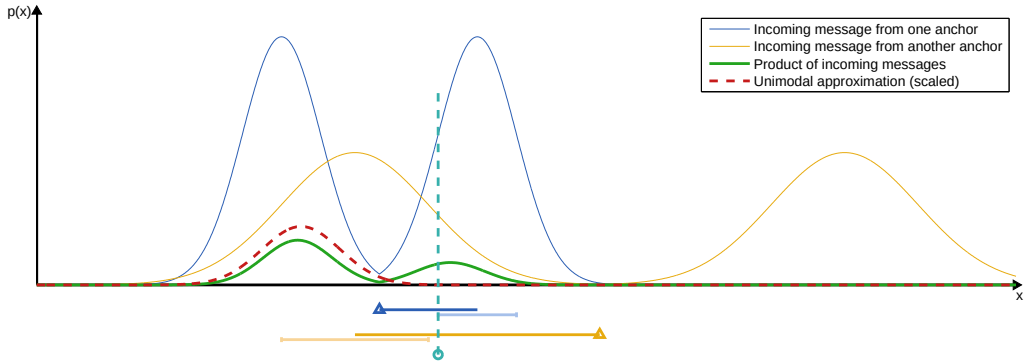

Figure 3.2: Example of a bimodal unconstrained message in 1D. The graph shows examples of messages from anchor nodes (see eq. (2.15)). The green line shows how the product of these messages might become bimodal. The two distance measurements and their ± 1 standard deviation are shown below the graph. An example of the true position of the mobile node is shown with a vertical dashed line.

This problem of bimodal unconstrained messages can also be shown for a 2D case. Figure 3.3(a) show an example of $\tilde{p}_r(\boldsymbol{x}_r)$ where a mobile node is connected to three anchor nodes with non-faulty distance measures of each link. The circular symmetric Gaussian with the least KL-divergence from $\tilde{p}_r(\boldsymbol{x}_r)$ is shown in 3.3(b). From this figure it is clear that in such a case the approximation is quite good.

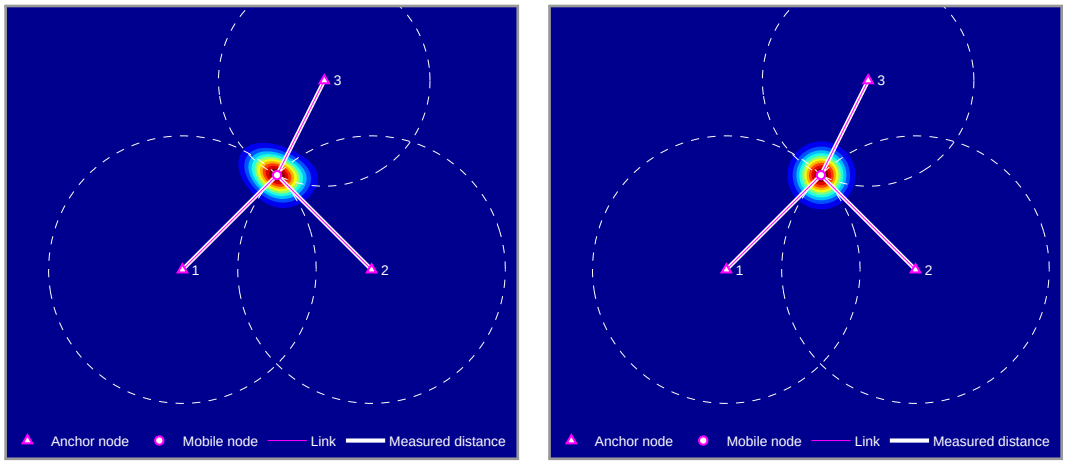

(a) (b)

Figure 3.3: Example with good distance measurements. With (a) $\tilde{p}_r(\boldsymbol{x}_r)$ and (b) $q_r'(\boldsymbol{x}_r) \in \mathcal{G}$.

However in the case that one or more distance measures are not perfect $\tilde{p}_r(\boldsymbol{x}_r)$ might have a form that is not unimodal. Figure 3.4(a) shows an example that is similar to Figure 3.3(a) but where the distance between anchor node 3 and the mobile node is reported to be longer that true distance and have a larger distance measurement variance. Approximating this $\tilde{p}_r(\boldsymbol{x}_r)$ with a unimodal circular symmetric Gaussian results in Figure

3.4(b). From this it is clear the strongest mode is chosen by the approximation, and that the less probable (but correct) mode is completely discarded.

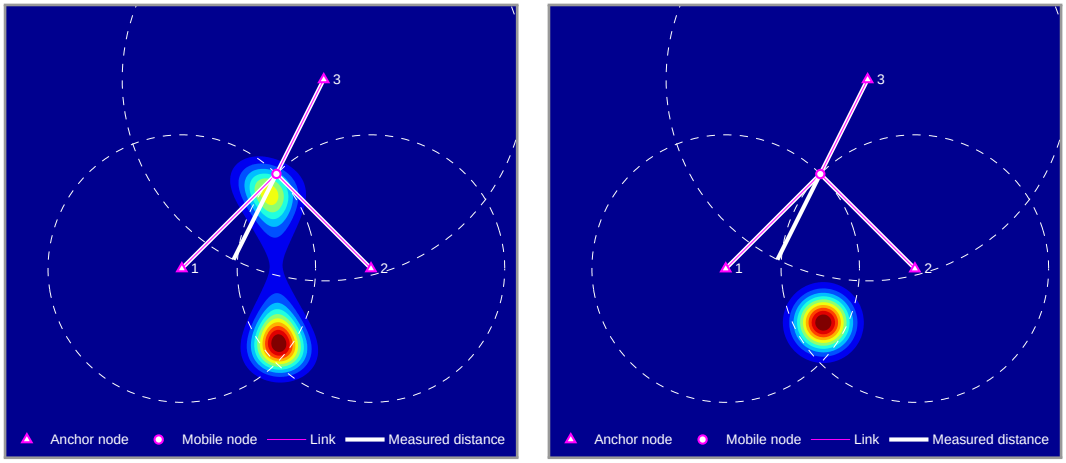

(a) (b)

Figure 3.4: Example with a bad distance measurement and unimodal approximation. With (a) $\tilde{p}_r(\boldsymbol{x}_r)$ and (b) $q'_r(\boldsymbol{x}_r) \in \mathcal{G}$.

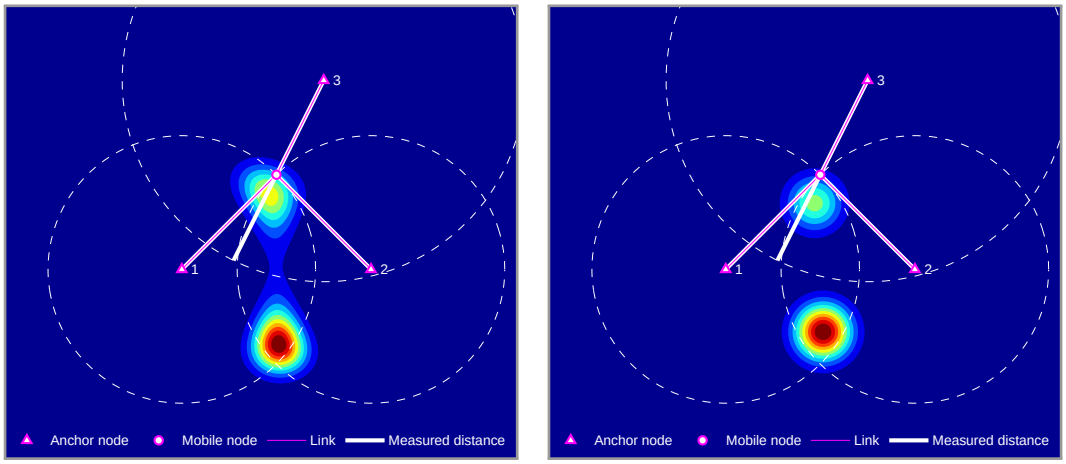

(a) (b)

Figure 3.5: Example with a bad distance measurement and bimodal approximation. With (a) $\tilde{p}_r(\boldsymbol{x}_r)$ and (b) $q'_r(\boldsymbol{x}_r) \in \mathcal{MG}$.

To improve the result of the algorithm it is proposed to approximate $\tilde{p}_r(\boldsymbol{x}_r)$ with a mixture of two circular symmetric Gaussians. We denote this family as $\mathcal{MG}$ (Mixture of Gaussians). An example of this is shown in Figure 3.5(b) where it is clear that the less probable mode is preserved if $q'_r(\boldsymbol{x}_r) \in \mathcal{MG}$.

The main idea of this improved approximation of $\tilde{p}_r(\boldsymbol{x}_r)$ with possibly two modes is to hopefully make it possible for neighbouring mobile nodes to more accurately or within fewer iterations find a good position estimate. Another benefit of the bimodal approximation is that odd shaped $\tilde{p}_r(\boldsymbol{x}_r)$ can be represented better.

It is however not trivial to predict how such a refinement will influence the localization performance of the algorithm. It depends on the localization scenario at hand and whether bimodal or oddly shaped unconstrained messages occur.

The implications of extending the algorithm to use a bimodal constraint over a unimodal constraint are rather limited due to the structure of the VMP algorithm. Besides the task of finding a new closed form expression for the KL-divergence and choosing a method for minimizing this, the extension only affects the algorithm in the sense that the size of the messages passed from the mobile nodes increases. With the circular symmetric Gaussian constraint the messages have contain the mean and variance (3 real values - assuming a 2-dimensional case) whereas for a mixture of two circular symmetric Gaussians 7 real values should be passed (1 ratio value (weight), 2 means, and 2 variances).

Section 3.1 describes the derivation of the closed form expression for the bimodal KL-divergence and the effect of this extension of the algorithm is presented in Chapter 5.

3.1 Closed form expression for the KL-divergence

The approximation $q'_r(\boldsymbol{x}_r)$ can be defined as a mixture of circular symmetric Gaussians where:

$$q'_r(\boldsymbol{x}_r) = \sum_{k=1}^{K} \dot{w}_{r,k}\, \mathcal{N}(\boldsymbol{x}_r \mid \dot{\boldsymbol{\mu}}_{r,k}, \dot{\sigma}^2_{r,k}) \tag{3.1}$$

with the constraint:

$$\sum_{k=1}^{K} \dot{w}_{r,k} = 1 \tag{3.2}$$

In the bimodal case of $K = 2$, which we want to implement, (3.1) and (3.2) reduces to:

$$q'_r(\boldsymbol{x}_r) = \dot{w}_{r,1}\, \mathcal{N}(\boldsymbol{x}_r \mid \dot{\boldsymbol{\mu}}_{r,1}, \dot{\sigma}^2_{r,1}) + (1 - \dot{w}_{r,1})\, \mathcal{N}(\boldsymbol{x}_r \mid \dot{\boldsymbol{\mu}}_{r,2}, \dot{\sigma}^2_{r,2}) \tag{3.3}$$

However as the definition in (3.1) is more generic and in some sense simpler it will be used throughout this derivation. The derivation follows the same steps as the derivation for the unimodal KL-divergence. See Section 2.1 for details. As for the unimodal case the KL-divergence can be written as:

$$\mathrm{KL}\left(q'_r(\boldsymbol{x}_r) \parallel \tilde{p}_r(\boldsymbol{x}_r)\right) \propto \mathrm{KL}\left(q'_r(\boldsymbol{x}_r) \parallel \mathcal{N}(\boldsymbol{x}_r \mid \tilde{\boldsymbol{\mu}}_r, \tilde{\sigma}^2_r)\right) \tag{3.4a}$$

$$- \sum_{a \in \mathcal{N}_r \cap \mathcal{N}_A} \mathbb{E}_{\boldsymbol{x}_r}\left[\ln \mathcal{N}(d_{r,a} \mid ||\boldsymbol{x}_r - \boldsymbol{\mu}_a||, \sigma^2_{d_{r,a}})\right] \tag{3.4b}$$

$$- \sum_{m \in \mathcal{N}_r \cap \mathcal{N}_M} \mathbb{E}_{\boldsymbol{x}_r}\left[\mathbb{E}_{\boldsymbol{x}_m}\left[\ln \mathcal{N}(d_{r,m} \mid ||\boldsymbol{x}_r - \boldsymbol{x}_m||, \sigma^2_{d_{r,m}})\right]\right] \tag{3.4c}$$

However contrary to the unimodal case no closed form expression exist for the first part (3.4a) when $q'_r(\boldsymbol{x}_r)$ is a mixture of Gaussians. Multiple approximations of the KL-divergence between two mixtures of Gaussians have been compared in [13], and of these "the variational approximation" is recommended. For two Gaussian mixtures f and g with components f_i and g_i having weights $w_{f,i}$ and $w_{g,i}$ this approximation is defined as:

$$\mathrm{D}_{\mathrm{var}}(f \parallel g) = \sum_a w_{f,a} \ln \frac{\sum_b w_{f,b} \exp(-\mathrm{KL}(f_a \parallel f_b))}{\sum_c w_{g,c} \exp(-\mathrm{KL}(f_a \parallel g_c))} \tag{3.5}$$

In our case where the prior knowledge is a single circular symmetric Gaussian (or "mixture" of one component) the KL-divergence can be stated as:

$$\mathrm{KL}\left(q_r'(\boldsymbol{x}_r) \parallel \mathcal{N}(\boldsymbol{x}_r \mid \tilde{\boldsymbol{\mu}}_r, \tilde{\sigma}_r^2)\right) \approx \mathrm{D}_{\mathrm{var}}\left(q_r'(\boldsymbol{x}_r) \parallel \mathcal{N}(\boldsymbol{x}_r \mid \tilde{\boldsymbol{\mu}}_r, \tilde{\sigma}_r^2)\right) = \sum_{k=1}^{K} \dot{w}_{r,k} \ln \frac{\sum_{l=1}^{K} \dot{w}_{r,l} \exp\left(-\frac{\dot{\sigma}_{r,k}^2}{\dot{\sigma}_{r,l}^2} - \frac{\left|\left|\dot{\boldsymbol{\mu}}_{r,k} - \dot{\boldsymbol{\mu}}_{r,l}\right|\right|^2}{2\dot{\sigma}_{r,l}^2} + 1 + \ln \frac{\dot{\sigma}_{r,k}^2}{\dot{\sigma}_{r,l}^2}\right)}{\exp\left(-\frac{\dot{\sigma}_{r,k}^2}{\tilde{\sigma}_r^2} - \frac{\left|\left|\dot{\boldsymbol{\mu}}_{r,k} - \tilde{\boldsymbol{\mu}}_r\right|\right|^2}{2\tilde{\sigma}_r^2} + 1 + \ln \frac{\dot{\sigma}_{r,k}^2}{\tilde{\sigma}_r^2}\right)} \tag{3.6}$$

For (3.4b) and (3.4c) the same approach as for the unimodal case can be used by noting that:

$$\mathbb{E}_{\boldsymbol{x}_r}\left[h(\boldsymbol{x}_r)\right] = \sum_{k=1}^{K} \dot{w}_{r,k}\, \mathbb{E}_{\boldsymbol{x}_{r,k}}\left[h(\boldsymbol{x}_{r,k})\right] \tag{3.7}$$

with $\boldsymbol{x}_{r,k} \sim \mathcal{N}(\dot{\boldsymbol{\mu}}_{r,k}, \dot{\sigma}_{r,k}^2)$. So the contribution from the neighbouring anchor nodes becomes:

$$\mathbb{E}_{\boldsymbol{x}_r}\left[\ln \mathcal{N}(d_{r,a} \mid ||\boldsymbol{x}_r - \boldsymbol{\mu}_a||, \sigma_{d_{r,a}}^2)\right] = \tag{3.8}$$

$$\ln \frac{1}{\sqrt{2\pi\sigma_{d_{r,a}}^2}} - \frac{d_{r,a}^2 - 2d_{r,a}\sum_{k=1}^{K} \dot{w}_{r,k}\, \mathbb{E}_{\boldsymbol{x}_{r,k}}\left[||\boldsymbol{x}_{r,k} - \boldsymbol{\mu}_a||\right] + \sum_{k=1}^{K} \dot{w}_{r,k}\, \mathbb{E}_{\boldsymbol{x}_{r,k}}\left[||\boldsymbol{x}_{r,k} - \boldsymbol{\mu}_a||^2\right]}{2\sigma_{d_{r,a}}^2} \tag{3.9}$$

Inserting the derived expressions for $\mathbb{E}_{\boldsymbol{x}_{r,k}}\left[||\boldsymbol{x}_{r,k} - \boldsymbol{\mu}_a||\right]$ and $\mathbb{E}_{\boldsymbol{x}_{r,k}}\left[||\boldsymbol{x}_{r,k} - \boldsymbol{\mu}_a||^2\right]$ (see eq. (2.25) and (2.28)) and grouping all constant terms into c this becomes:

$$\begin{aligned}\mathbb{E}_{\boldsymbol{x}_r}\left[\ln \mathcal{N}(d_{r,a} \mid ||\boldsymbol{x}_r - \boldsymbol{\mu}_a||, \sigma_{d_{r,a}}^2)\right] = \\ -\frac{1}{2\sigma_{d_{r,a}}^2}\left[-2d_{r,a}\sum_{k=1}^{K} \dot{w}_{r,k}\sqrt{\dot{\sigma}_{r,k}^2 \tfrac{\pi}{2}}\, \mathrm{M}\left(-\frac{1}{2}, 1, -\frac{\left|\left|\dot{\boldsymbol{\mu}}_{r,k} - \boldsymbol{\mu}_a\right|\right|^2}{2\dot{\sigma}_{r,k}^2}\right)\right. \\ \left. + \sum_{k=1}^{K} \dot{w}_{r,k}\left(\left|\left|\dot{\boldsymbol{\mu}}_{r,k} - \boldsymbol{\mu}_a\right|\right|^2 + 2\dot{\sigma}_{r,k}^2\right)\right] + c \end{aligned} \tag{3.10}$$

$$\begin{aligned}= -\frac{1}{2\sigma_{d_{r,a}}^2}\sum_{k=1}^{K} \dot{w}_{r,k}\left[-2d_{r,a}\sqrt{\dot{\sigma}_{r,k}^2 \tfrac{\pi}{2}}\, \mathrm{M}\left(-\frac{1}{2}, 1, -\frac{\left|\left|\dot{\boldsymbol{\mu}}_{r,k} - \boldsymbol{\mu}_a\right|\right|^2}{2\dot{\sigma}_{r,k}^2}\right)\right. \\ \left. + \left|\left|\dot{\boldsymbol{\mu}}_{r,k} - \boldsymbol{\mu}_a\right|\right|^2 + 2\dot{\sigma}_{r,k}^2\right] + c \end{aligned} \tag{3.11}$$

For the contributions from the neighbouring mobile nodes we can again use that:

$$\mathbb{E}_{\boldsymbol{x}_r}\left[\mathbb{E}_{\boldsymbol{x}_m}\left[h(\boldsymbol{x}_r, \boldsymbol{x}_m)\right]\right] = \sum_{k=1}^{K}\sum_{l=1}^{K} \dot{w}_{r,k}\hat{w}_{m,l}\, \mathbb{E}_{\boldsymbol{x}_{r,k}}\left[\mathbb{E}_{\boldsymbol{x}_{m,l}}\left[h(\boldsymbol{x}_{r,k}, \boldsymbol{x}_{m,l})\right]\right] \tag{3.12}$$

Hence the same principles as for the unimodal case can be used. Grouping constant terms into c the contribution from each neighbouring mobile node can be expressed as:

$$\begin{aligned}
&\mathbb{E}_{\boldsymbol{x}_r}\left[\mathbb{E}_{\boldsymbol{x}_m}\left[\ln \mathcal{N}(d_{r,m} \mid ||\boldsymbol{x}_r - \boldsymbol{x}_m||, \sigma^2_{d_{r,m}})\right]\right] = \\
&\quad -\frac{1}{2\sigma^2_{d_{r,m}}}\left[-2d_{r,m}\sum_{k=1}^{K}\sum_{l=1}^{K}\dot{w}_{r,k}\hat{w}_{m,l}\sqrt{(\dot{\sigma}^2_{r,k}+\hat{\sigma}^2_{m,l})\tfrac{\pi}{2}}\,\mathrm{M}\left(-\frac{1}{2},1,-\frac{||\dot{\boldsymbol{\mu}}_{r,k}-\hat{\boldsymbol{\mu}}_{m,l}||^2}{2(\dot{\sigma}^2_{r,k}+\hat{\sigma}^2_{m,l})}\right)\right. \\
&\qquad\qquad \left. +\sum_{k=1}^{K}\sum_{l=1}^{K}\dot{w}_{r,k}\hat{w}_{m,l}\left(||\dot{\boldsymbol{\mu}}_{r,k}-\hat{\boldsymbol{\mu}}_{m,l}||^2+2\dot{\sigma}^2_{r,k}\right)\right]+c \qquad (3.13) \\
&= -\frac{1}{2\sigma^2_{d_{r,m}}}\sum_{k=1}^{K}\sum_{l=1}^{K}\dot{w}_{r,k}\hat{w}_{m,l}\left[-2d_{r,m}\sqrt{(\dot{\sigma}^2_{r,k}+\hat{\sigma}^2_{m,l})\tfrac{\pi}{2}}\,\mathrm{M}\left(-\frac{1}{2},1,-\frac{||\dot{\boldsymbol{\mu}}_{r,k}-\hat{\boldsymbol{\mu}}_{m,l}||^2}{2(\dot{\sigma}^2_{r,k}+\hat{\sigma}^2_{m,l})}\right)\right. \\
&\qquad\qquad \left. +||\dot{\boldsymbol{\mu}}_{r,k}-\hat{\boldsymbol{\mu}}_{m,l}||^2+2\dot{\sigma}^2_{r,k}\right]+c \qquad (3.14)
\end{aligned}$$

Inserting (3.6), (3.11), and (3.14) into (3.4) while ignoring the constant terms gives the closed form expression to be minimized for the multimodal case. To do the numerical minimization a closed form expression for the gradient is found as well. This is shown in Appendix B. With this closed form expression for the bimodal KL-divergence the implementation of the extented VMP algorithm is straightforward.

4 Implementation

This chapter presents some of the things to consider when implementing a real world cooperative localization algorithm. These considerations help define a common framework with a flexible structure for testing the two algorithms VMP and B-VMP.

As mentioned in Chapter 1 it is essential to decide whether the algorithm should be run in centralized or distributed localization scheme. For this work we assume that a distributed scheme is selected upon and will hence describe the arising challenges from this choice.

The straight-forward definition of the VMP algorithm in Algorithm 1 on page 9 gives a simple recipe for performing localization. However this definition does not specify anything about when, how, and whom can or should invoke the algorithm for performing the localization. Furthermore it does not specify how the distance measurements should be obtained and how the communication between the nodes should be handled. It as well does not specify a stopping criterion.

Participation of mobile nodes in cooperative localization

In the case of non-cooperative localization the localization algorithm can be invoked whenever the mobile node find it convenient. E.g. for GPS-based navigation the localization algorithm could be invoked at a fixed time interval or based on measurements from inertial sensors. But in the case of cooperative localization this task of invoking a localization procedure becomes bit more complicated.

Performing cooperative localization requires some effort of the neighbouring nodes as they would have to perform distance measurements and possibly computations for the localization algorithm to run. This effort costs both computation time and energy for the neighbouring nodes. But for mobile nodes these resources are likely limited and hence the neighbouring nodes would have to somehow decide whether to participating in this cooperative localization procedure or not. E.g. if a mobile node only have a small amount of battery power left and does not need a new position update for itself it might choose not to participate in a cooperative localization procedure initiated by another mobile node on the network. The scale of this problem of course depends on the application at hand, e.g. it might be a problem for individual smartphones in an office network whereas for a cooperative sensor network with a common goal it might be less of a problem.

To simplify the implementation and testing of the algorithms this decision of invoking the procedure is simply generalized and termed a “position request”. When, how, and whom initiates a position request is not important to the algorithm as such but the way the mobile nodes choose to participate is.

Node communication

In a distributed iterative cooperative localization algorithm it is important that the mobile nodes can communicate. However it is not important how the nodes communicate. This could be via a common network or by peer-to-peer connections. The important thing to notice is that the communication between the nodes might not be perfect, and the communication link between two nodes might be unreliable or stop working during the

iterative procedure. It is therefore important that the testing framework can handle and simulate such losses of communication. In the case of a message from one mobile node to another does not arrive at an iteration step it is then up to the algorithm to decide if it should discard all information from this node or assume that the content of the last message is still valid. In the case of the (B-)VMP algorithm this might even be exploited as a feature that a mobile node could choose to not send a message if it is identical to the previous message broadcasted or is within a small numerical boundary hereof.

In any case it is important to define some communication scheme to determine when a message is considered lost, e.g. due to a fixed timeout setting. Such a timeout setting depend on the application at hand and should besides communication delay allow for reasonable amount of time to collect incoming messages and compute an outgoing message.

Stopping criterion

Determining when to stop the iterative algorithm depends on multiple factors. One consideration could be that the mobile nodes might have moved and hence a new position request should be made with new fresh distance measurements. For some applications it might be beneficial to abort the algorithm before it has converged and do a new position request. For other applications the opposite might be true.

If no new urgent distance measurements are required, e.g. if the mobile nodes are assumed to be static, the algorithm would have to terminate based on some other criterion. A simplistic way to do this would be a fixed number of iterations. But determining such a one-size-fits-all number is not trivial. A dynamic approach on the other hand would allow the algorithm to terminate quickly if it has already converged. One way to do so would be to look at the difference of the between the current and previous computed outgoing message (mean, variance, and weight). If all mobile nodes reported "no change" then the algorithm could be terminated by assuming that the algorithm has converged to its best set of position estimates.

Obtaining distance measurements

Another consideration is how to obtain the distance measurements between the nodes. As presented in Chapter 1 multiple technologies and methods exists for obtaining a distance estimate. However as the accuracy of the distance estimates have directly influence on the localization results it is important that they are as accurate as possible. Furthermore for (B-)VMP algorithm it is important that an estimate of the distance error variance is provided as well. A simple approach to this is to measure the distance multiple times and hope that the fluctuations in the measurements are representative for the true distance error variance. Note that this distance error variance should encompass the true distance error, i.e. including offset caused by NLOS conditions.

In a static environment this might be a problem as two nodes could measure the exact same distance over and over again even if this is a non-direct path. This would result in a measured variance of zero which of course would not be representative if the distance measured is a non-direct path that is much longer that the true direct distance.

One solution to this problem is to measure the distance using multiple radio access technologies (RAT). If two nodes both support multiple RATs that operates with different frequency characteristics this might result in different distance estimates due to the dif-

ferent propagation properties. Fusing such two distance measurements to a hybrid RAT distance measurement might give a better estimate of the distance as well as the distance error variance. For RATs with multiple channels available this could also be achieved by measuring the distance using each channel.

If the RAT available uses Ultra WideBand (UWB) communication this might already be somewhat exploited due to the large bandwidth that makes it possible to identify multipath components and hence better determine the LOS component [14].

Another practical consideration regarding obtaining the distance measurements is to determine the time allowed for performing these measurements.

4.1 Algorithm implementation

With the considerations above in mind a common framework for the two algorithms have been implemented. The main purpose of this framework is to investigate the behaviour of the two algorithms. So besides the flexibility needed to handle the above considerations the framework is as well designed to save all intermediate values for subsequent analysis, e.g. all passed messages. Fortunately the structure of the (B-)VMP algorithm is relatively simple and straight-forward to implement.

The purpose of this section is not explain the trivial details of the implementation but rather the flexible structure of the data that permits the implementation to be used for both simulations and testing on real measurement data.

The input to the algorithm is represented with a MATLAB structure of the following format:

`scenario`

- `.name`: Name of the input scenario.
- `.map`: Structure with image of floor plan for plotting the results.
- `.nodes`: Structure array with the nodes.
  - `.node_id`
  - `.name`
  - `.anchor`: Boolean value to indicate anchor node.
- `.position_requests`: Structure array with data of all position requests.
  - `.timestamp`
  - `.true_positions`: Structure array with true position for all nodes for this position request. The true position of anchor nodes are used in the algorithm whereas true position for mobile nodes are only used for evaluation.
    - `.node_id`
    - `.x`
    - `.y`
  - `.distance_estimates`: Structure array for distance estimates.
    - `.node_id_a`
    - `.node_id_b`

`.distance`

`.distance_variance`

The choice of using MATLAB structures compared to simple matrices is due to readability concerns for the source code of the algorithm. For real world measurements the structure as well contain the link measurements used to the generate the distance estimates. This way all data related to a scenario is contained within one variable and the structure can handle both simulated data and real world measurements.

The implementation of the (B-)VMP algorithm follows the basis form presented in Algorithm 1 on page 9. For each iteration a structure is created (and saved) that contains all incoming messages. The content of this structure is then used to create a function handle to the closed form expression of the KL-divergence with this data inserted. This function handle is passed to MATLAB's `GlobalSearch` algorithm from the Global Optimization Toolbox for determining the global minimum of this function. The global optimization procedure is initiated with the parameters estimates found in the previous iteration. The `GlobalSearch` algorithm has a default value of 1000 for `NumTrialPoints` which defines the number of potential starting points for algorithm. However it was observed that this number in most cases could be reduced to 250 without affecting the results but giving a significant computational saving. So where nothing else is specified the algorithm uses `NumTrialPoints = 250`.

The main part of the algorithm can be found in ▶`/matlab/vmp_algorithm.m`, and the closed form expression for the KL-divergence for VMP and B-VMP can be found in ▶`/matlab/vmp_algorithm_kld_unimodal.m` and ▶`/matlab/vmp_algorithm_kld_bimodal.m`, respectively.

5 Results

The implementation of the two algorithms have been tested on two types of data; simulated scenarios and the real measurement data from the WHERE2 project. An initial implementation of the VMP algorithm was tested on simulated scenarios similar to those described in [1] with 13 anchor nodes and 100 mobile nodes. However to investigate the behaviour of the algorithms more closely a simpler scenario with fewer nodes have been defined. Section 5.1 describes this simple simulation scenario and some of the results that have been obtained from simulations using this scenario. Section 5.2 presents some results from the DLR preliminary measurement campaign from the WHERE2 project.

5.1 Simulations

To investigate the behaviour of both the VMP and B-VMP algorithm a simple simulation scenario has been constructed. This scenario was devised with two goals in mind: simplicity and flexibility. The simplicity is achieved by using only 3 anchor nodes and 10 mobile nodes. As the simulation scenario is intended for only 2-dimensional localization 3 anchor nodes is sufficient to avoid ambiguity caused by rotation or mirroring. The number of mobile nodes is chosen as a trade-off between having as few nodes as possible for simplicity while still having enough mobile nodes to generate interesting scenarios that depends on cooperation between the nodes to achieve good localization performance.

Figure 5.1 shows an example of the devised simulation scenario. This example will be used throughout this section. The simulation "floor plan" is a rectangle of 30×20 m. The mobile nodes are distributed uniformly and independently within this rectangle. The anchor nodes are located such that they do not form a isosceles triangle. This way it is easy to verify that the plotting of a generated scenario have not been mirrored in the process.

The simulated distances measures are generated by first deciding whether two nodes are connected and then making a noisy distance measurement. As in [10] the probability of two nodes being connected given their true distance d is defined as:

$$p(d) = \exp\left(\frac{-d^2}{2R^2}\right) \tag{5.1}$$

where R is the communication range. This gives a probability of a connection of roughly 88 % for $d = \frac{R}{2}$, 60 % for $d = R$, and 14 % for $d = 2R$. The parameter R adds flexibility to the simulation scenario. A large R would result in a well connected network while a small R would result in a scenario where each node only has a few connections. Compared to a fixed communication range this probabilistic approach to connectivity also add diversity to the generated scenarios.

The distance measurements can by generated in multiple ways to simulate some underlying RAT and distance measurement method. However for the results shown here the distance measures are generated by adding zero-mean Gaussian noise to the true distances. This is done to comply with the assumption from the algorithms so that the comparison is as fair as possible.

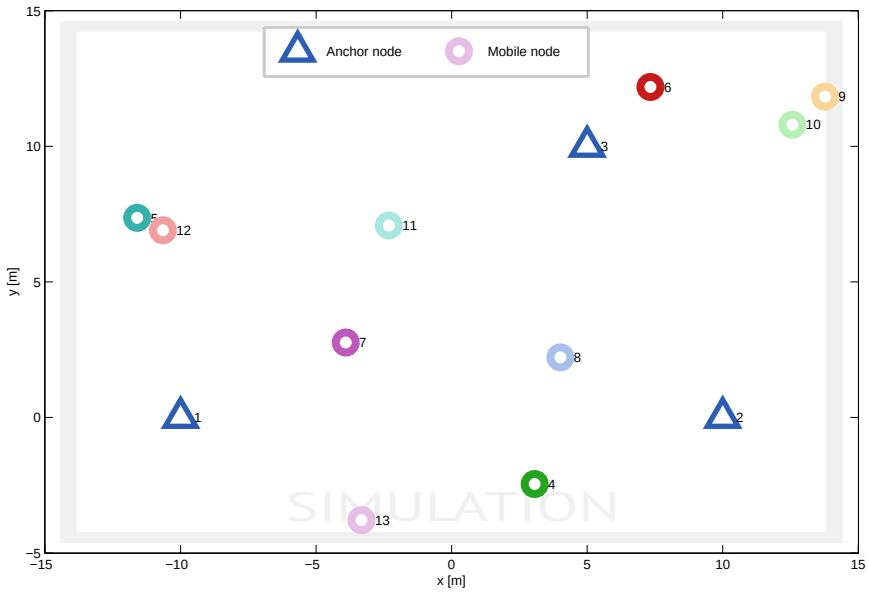

Figure 5.1: Example of the simple simulation scenario with 3 anchor nodes at fixed locations and 10 mobile nodes uniformly distributed within the boundaries.

Figure 5.2 shows an example of how these measurements might look like. Note that in this figure only the distance measurements from anchor nodes to mobile nodes are shown. These distance measurements are coloured to so that they match the colour of the mobile node. Figure 5.3 shows the full scenario including the cooperative mobile to mobile distance measurements. These cooperative measurements are shown in yellow.

From Figure 5.2 it is clear that this simple scenario can generate a diverse set of challenges for localization algorithms. This example shows how distance measurements can be way off and that some mobile nodes like node 8, 9, and 10 is only connected to one anchor. The example was generated with $R = 15$ m and a distance measurement error variance of $\sigma^2_{d_{r,t}} = 3$.

Figure 5.4(a) and 5.4(b) shows the resulting position estimates from the VMP and B-VMP algorithm, respectively. Both algorithms have been run for 15 iterations. From these results it is clear that the B-VMP algorithm in this specific case gives a better position estimate. While node 4, 7, and 8 are better positioned by the VMP algorithm the 7 other mobile nodes are worse positioned.

Figure 5.5(a) and 5.5(b) shows how the error of the position estimates converges for the two algorithms. For each iteration the position error for each mobile node is plotted as color indicating the size of the error. Note that the interpolation of colours between the data points only serve as a visual aid. From these plots it is also clear that the B-VMP algorithm handles this scenario better than the VMP algorithm.

This particular example is of course chosen to highlight the potential of the B-VMP algorithm. However explaining why this particular example is better suited for the B-VMP algorithm is not trivial since it depends on the interplay between the mobile nodes during the iterations of the algorithms. To shed some light on this matter the unconstrained $\tilde{p}_r(\boldsymbol{x}_r)$ have been plotted for all mobile nodes for the first 5 iterations for both algorithms. Figure 5.6 shows the result for VMP and Figure 5.7 for B-VMP. In these figures the true location of the mobile node is shown with a green dot and the selected

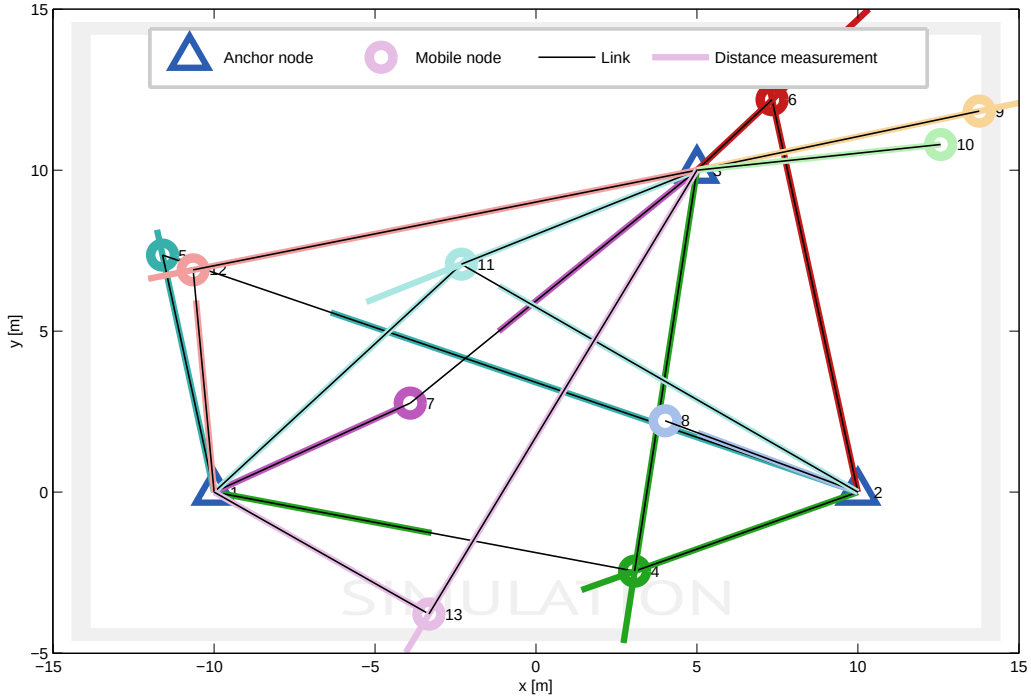

Figure 5.2: Example of simple simulation scenario with anchor to mobile distance measurements shown. The colour of the distance measurement is determined by the colour of the mobile node.

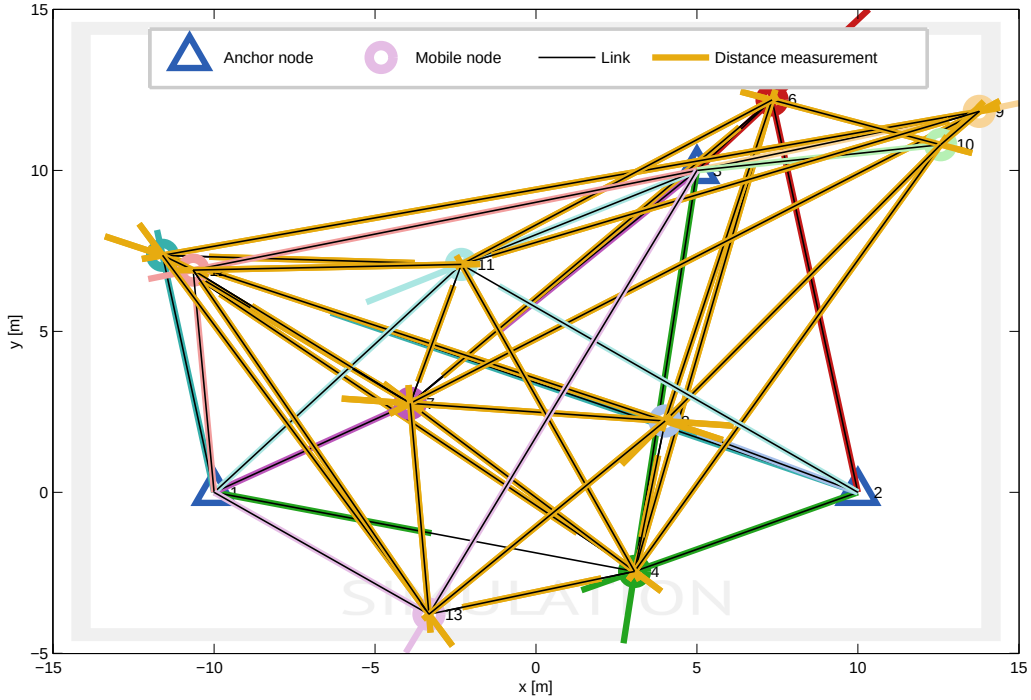

Figure 5.3: Same as Figure 5.2 but also showing the cooperative mobile to mobile distance measurements. These are shown in yellow.

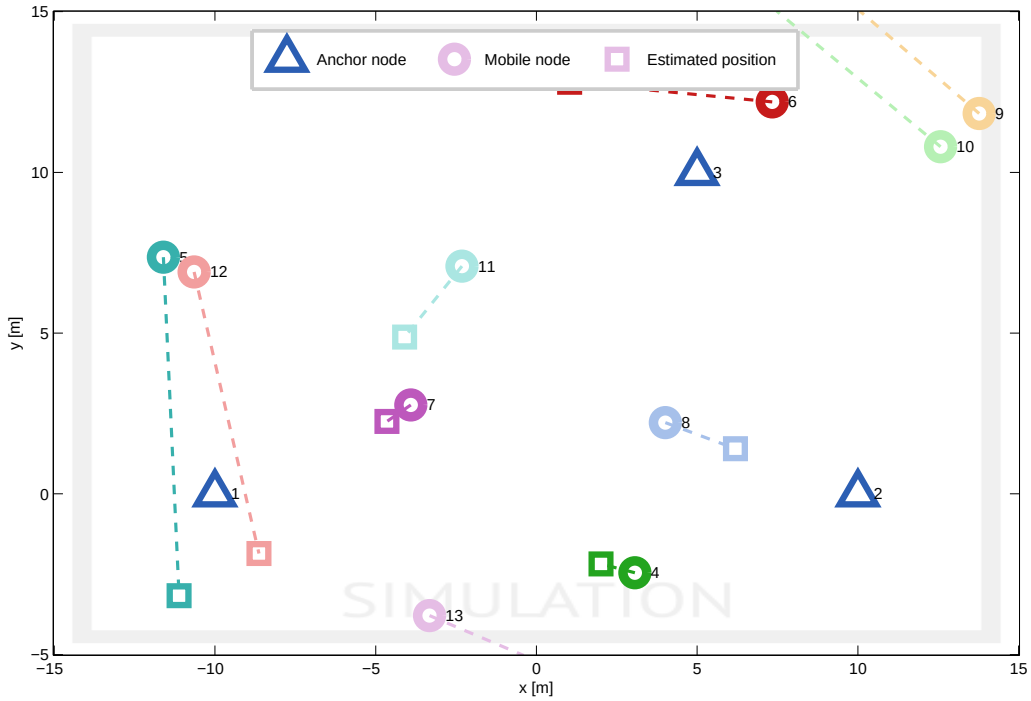

(a) VMP

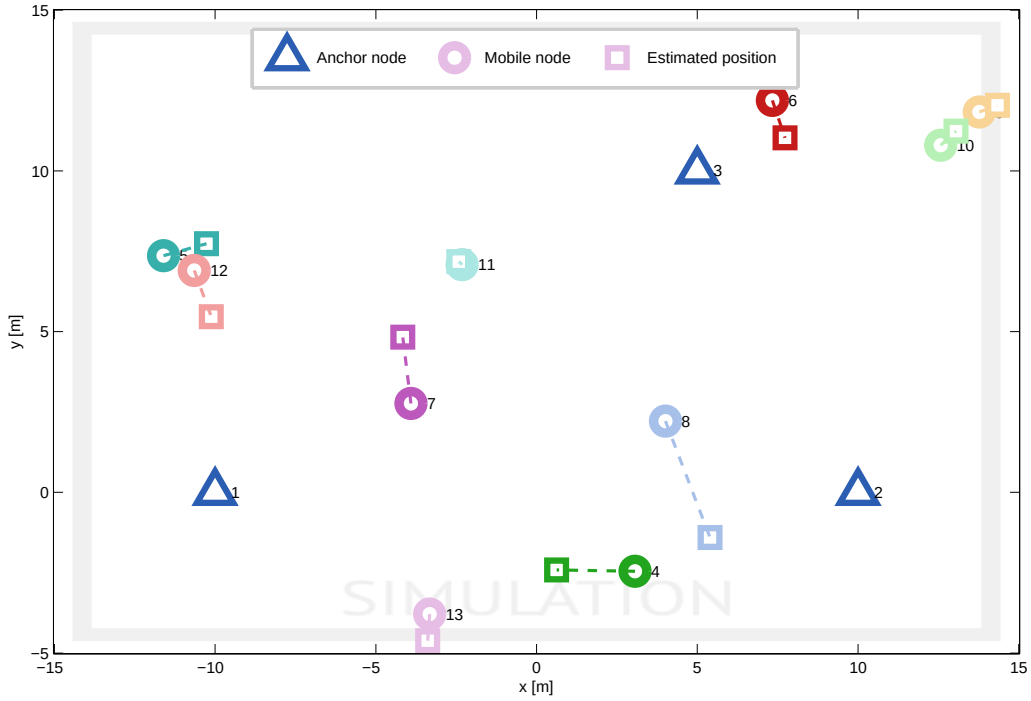

(b) B-VMP

Figure 5.4: Resulting position estimates by the two algorithms after 15 iterations.

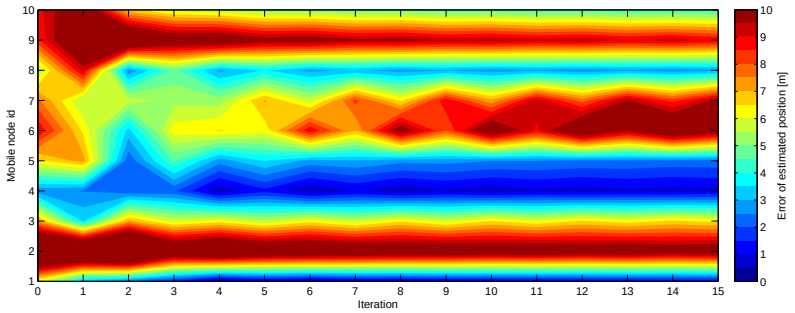

(a) VMP

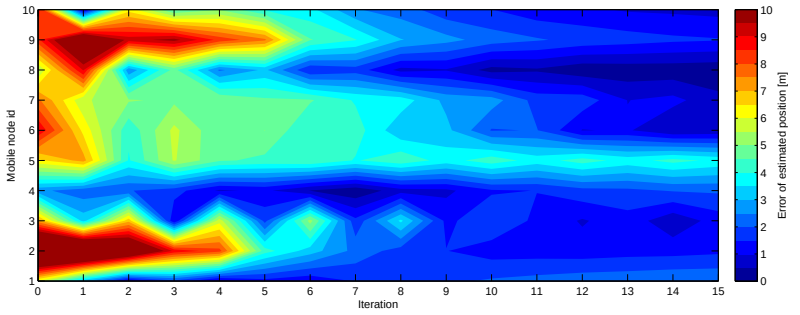

(b) B-VMP

Figure 5.5: Position estimate error for each mobile node for each iteration.

mean(s) of the circular symmetric Gaussian(s) is shown with an yellow circle. For the B-VMP plots the red square shows the weighted average of the two selected means, i.e. $\hat{w}_{r,1}\hat{\boldsymbol{\mu}}_{r,1} + (1 - \hat{w}_{r,1})\hat{\boldsymbol{\mu}}_{r,2}$. This weighted average is as well used as the position estimate for this iteration.

The $\tilde{p}_r(\boldsymbol{x}_r)$ messages are shown with coloured contours. The colours are used to distinguish them from each other and to pair them with the mobile node they represent. The colours used are the same as from the previous figures (see Figure 5.1), e.g. the red contour belongs to mobile node 6. The figures show a wide variety of shapes that the $\tilde{p}_r(\boldsymbol{x}_r)$ can take during the iterations of the algorithms. It is clear that $\tilde{p}_r(\boldsymbol{x}_r)$ is not always circular. It might be oblong, banana shaped, or some other irregular shape and it might be bimodal. From these figures it as well becomes apparent that the bimodal shape can occur from the changes of the approximated beliefs of the position estimates from the neighbouring nodes. Note that the variance of the Gaussian circular symmetric approximations are not shown. The changes in these variances contribute to generate bimodal shapes.

Figure 5.6(c) shows two examples where the VMP algorithm has to choose one mode of a bimodal $\tilde{p}_r(\boldsymbol{x}_r)$. Both the $\tilde{p}_r(\boldsymbol{x}_r)$ for mobile node 6 and 13 are bimodal (the non-chosen mode of 13 is the one to the left of the true position of mobile node 11). In Figure 5.7(c) in can be seen how B-VMP for both mobile node 5 and 6 has selected means that match the modes of the bimodal $\tilde{p}_r(\boldsymbol{x}_r)$.

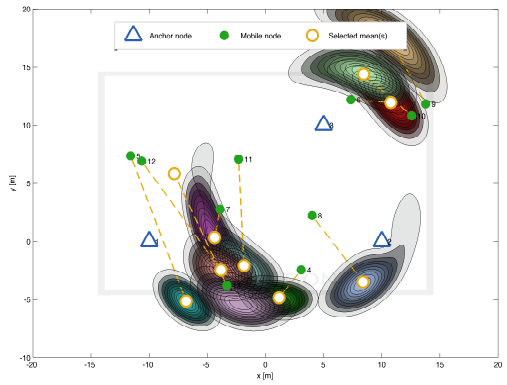

(a) VMP: Iteration 1

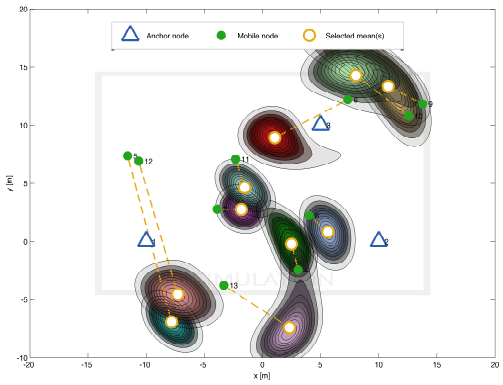

(b) VMP: Iteration 2

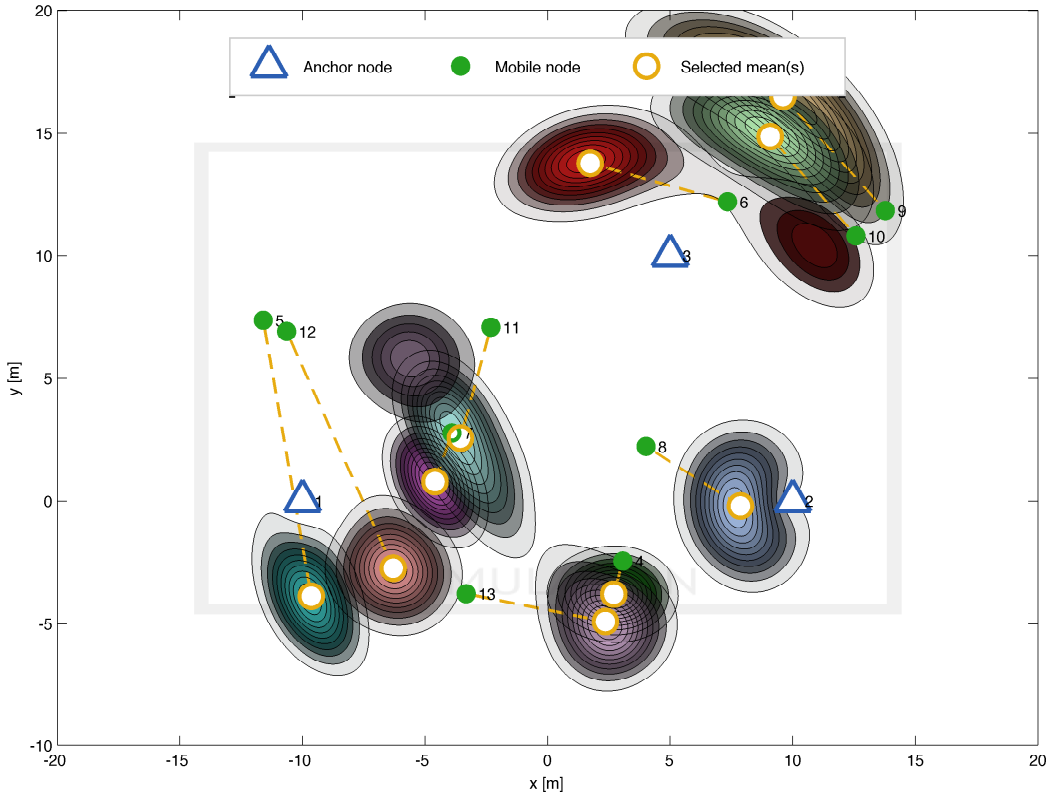

(c) VMP: Iteration 3

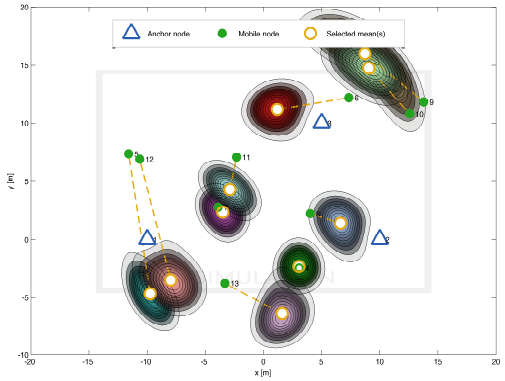

(d) VMP: Iteration 4

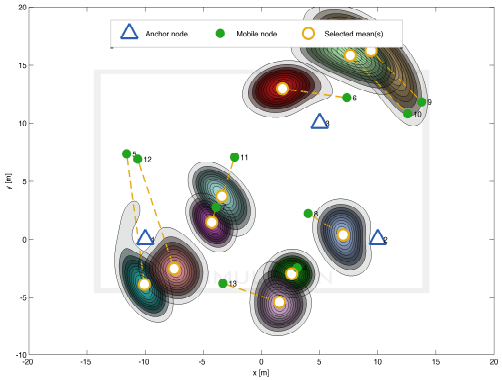

(e) VMP: Iteration 5

Figure 5.6: Map of $\tilde{p}_r(\boldsymbol{x}_r)$ for each mobile node for selected iterations. These are for the VMP algorithm.

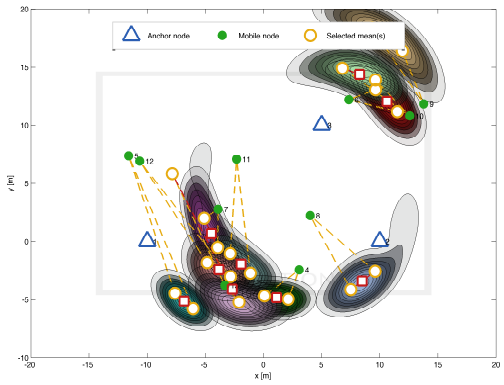

(a) B-VMP: Iteration 1

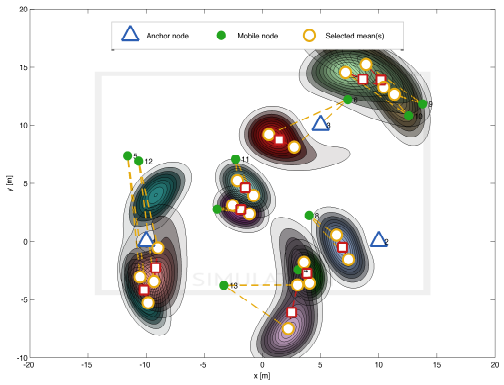

(b) B-VMP: Iteration 2

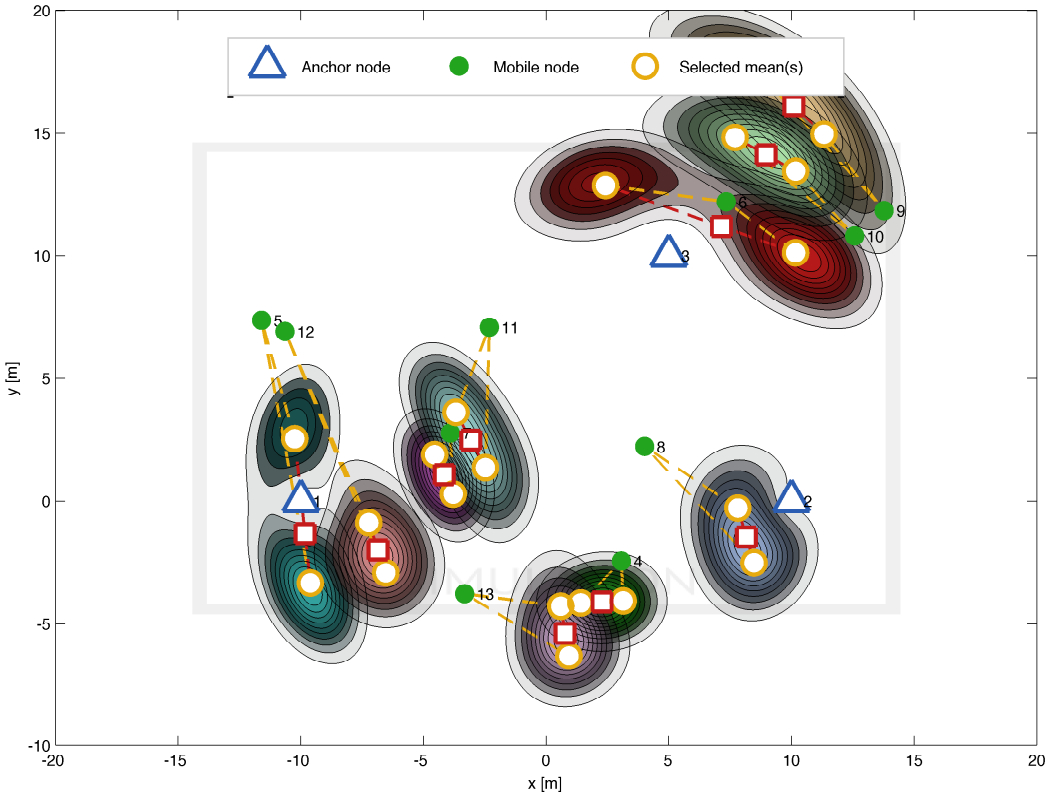

(c) B-VMP: Iteration 3

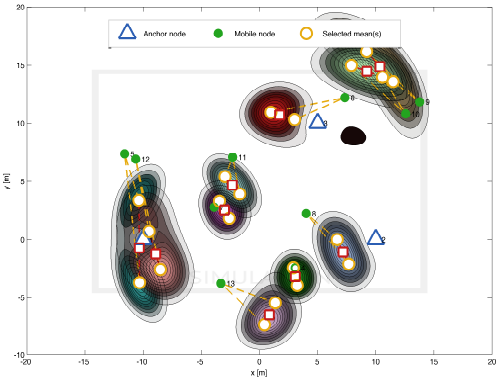

(d) B-VMP: Iteration 4

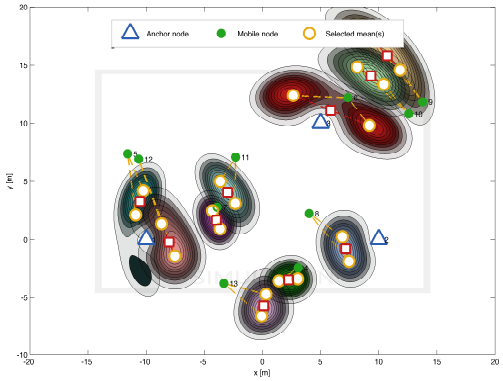

(e) B-VMP: Iteration 5

Figure 5.7: Map of $\tilde{p}_r(\boldsymbol{x}_r)$ for each mobile node for selected iterations. These are for the B-VMP algorithm.

5.1.1 Monte Carlo simulations

While the previous example show how the B-VMP algorithm can outperform VMP in a specific case the real interesting question is how often this is the case. To investigate this a set of Monte Carlo simulations have been conducted. The parameters used have been $R = \{10, 15\}$ and the distance measurement error variance $\sigma^2_{d_{r,t}} = \{1, 1.5, 2, 3, 5\}$. For each combination of these two parameters 200 scenarios have been generated and passed through the algorithms for 15 iterations. Figure 5.8(a) shows a CDF of position estimate errors for $R = 10$ and Figure 5.8(b) for $R = 15$. The solid lines are for the B-VMP algorithm and the dashed lines for the VMP algorithm. For $R = 10$ the average number of connections per node is 5.7 whereas for $R = 15$ it is 8.0. From Figure 5.8(a) it appears that B-VMP generally perform better for all settings of the distance measurement variance. This indicates that for these low connectivity scenarios with few anchors the B-VMP algorithm is beneficial and produces better position estimates. However for $R = 15$ it appears that there is only little or no improvement using B-VMP over VMP.

However these CDF plots does not show whether the individual nodes are generally located better or just differently. To investigate this histograms have been created that shows the difference in the position estimates for individual nodes between VMP and B-VMP. These are shown in Figure 5.9. The difference is calculated for each node as VMP position error minus B-VMP position error. Hence positive differences means that B-VMP result is better. Note that the plots are limited to 5 % to highlight the differences between the two algorithms. From Figure 5.9(a) it is clear that while the CDF indicates an general improvement this does not mean that all mobile nodes are located better. However the B-VMP result is better and 54.9 % of the mobile nodes have been located more accurately. 7.9 % of the nodes are located better than 2 m while only 4.9 % are located worse than -2 m (negative difference, VMP better). The case for $R = 15$ is shown in Figure 5.9(b) and only 51.6 % is located better with B-VMP. And for error differences larger than 2 m the percentage is just 2.7 % and for differences less than -2 m it is 2.5 %.

From these simulations it seems that the B-VMP algorithm is more beneficial the tougher the scenario, e.g. low connectivity and large distance measurement error variance. Of the simulated scenarios the one with the largest improvement by B-VMP vs. VMP is for $R = 10$ m and $\sigma^2_{d_{r,t}} = 3$. In this scenario the position estimate is improved for 57.6 % of the nodes, and for 8 % more than 2 m while only 3.8 % is less than -2 m.

Another thing to note is that for $R = 15$ m and $\sigma^2_{d_{r,t}} = 1$ the VMP algorithm seem to be notably better than the B-VMP. However as this seemed unintuitive it was investigated further and it turned out that the global optimization procedure did not find the global minimum but only a local minimum for some of the nodes. All simulations of Figure 5.8 was conducted with the the global optimization setting `NumTrialPoints` set to 250. To see the effect of this the scenario was re-run with `NumTrialPoints` set to 1000. Figure 5.10 shows the comparison of these two runs. From this figure it is clear that global optimization parameters had been set too low for this scenario.

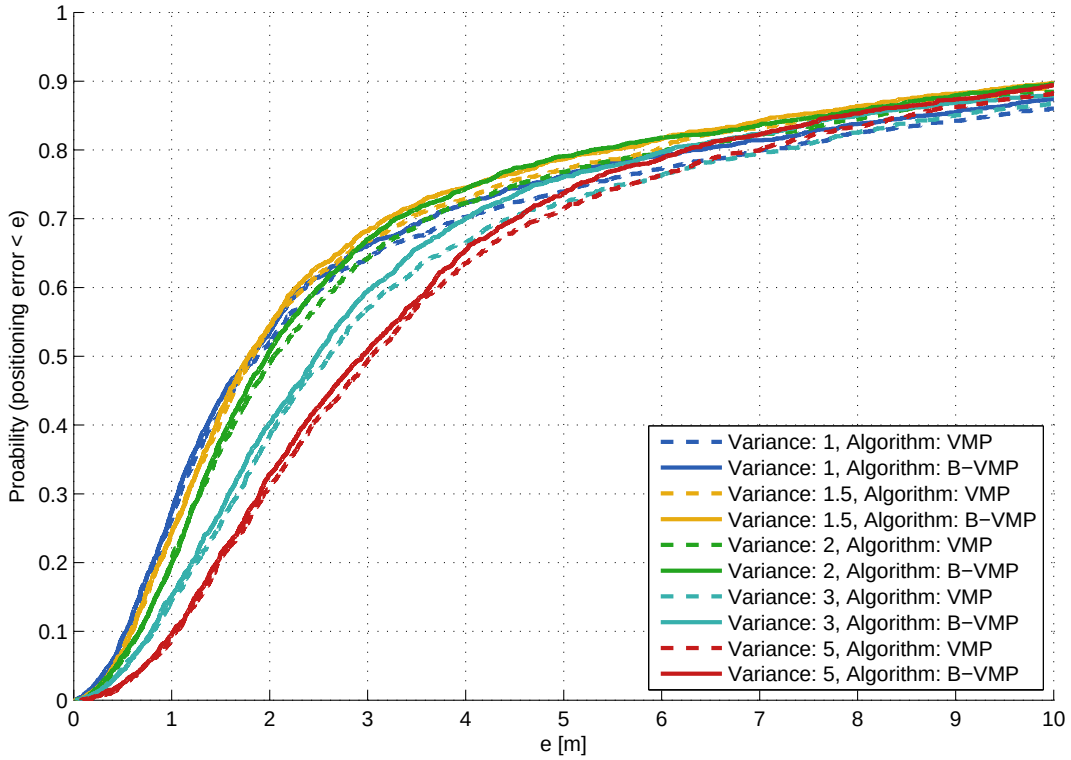

(a) $R = 10$ m

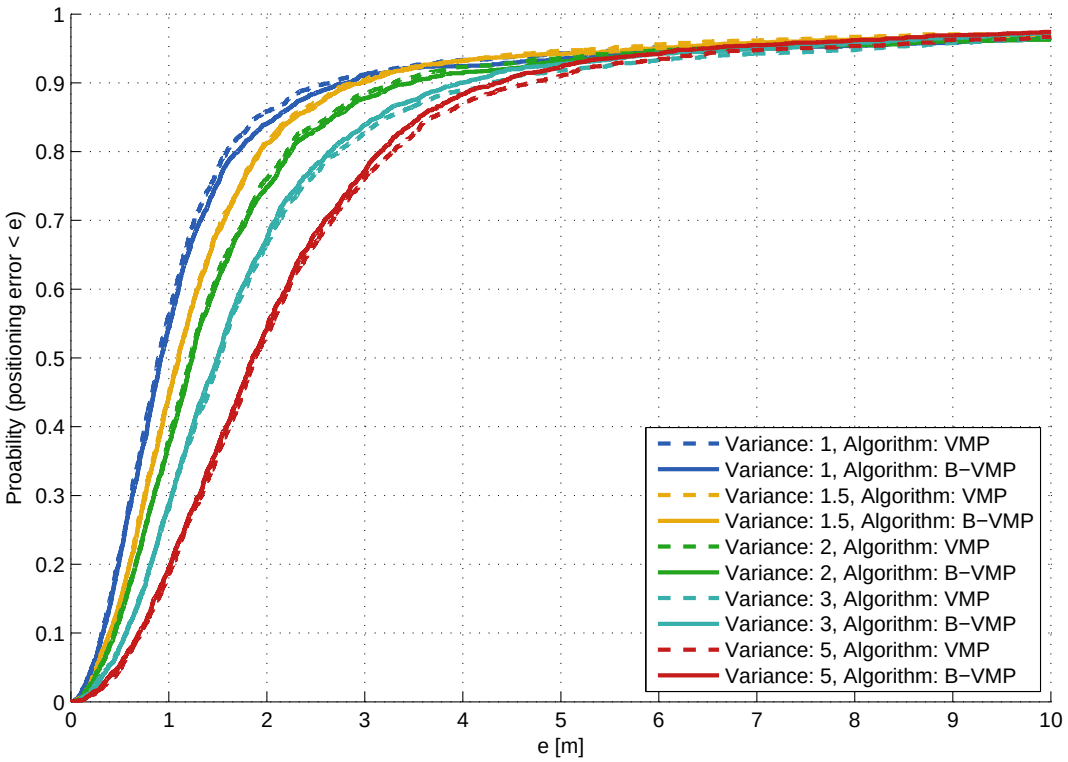

(b) $R = 15$ m

Figure 5.8: CDF of position errors for different sets of simulation parameters. See text for further description.

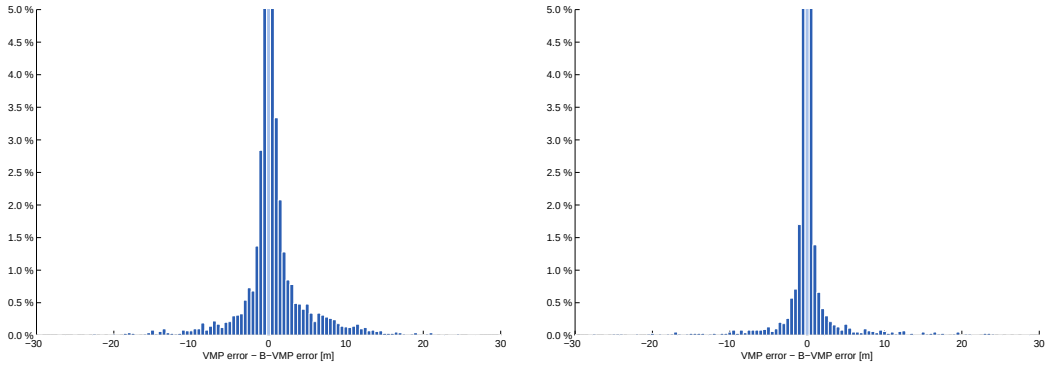

(a) $R = 10$ m (b) $R = 15$ m

Figure 5.9: Histogram showing the position error difference for VMP error minus B-VMP error.

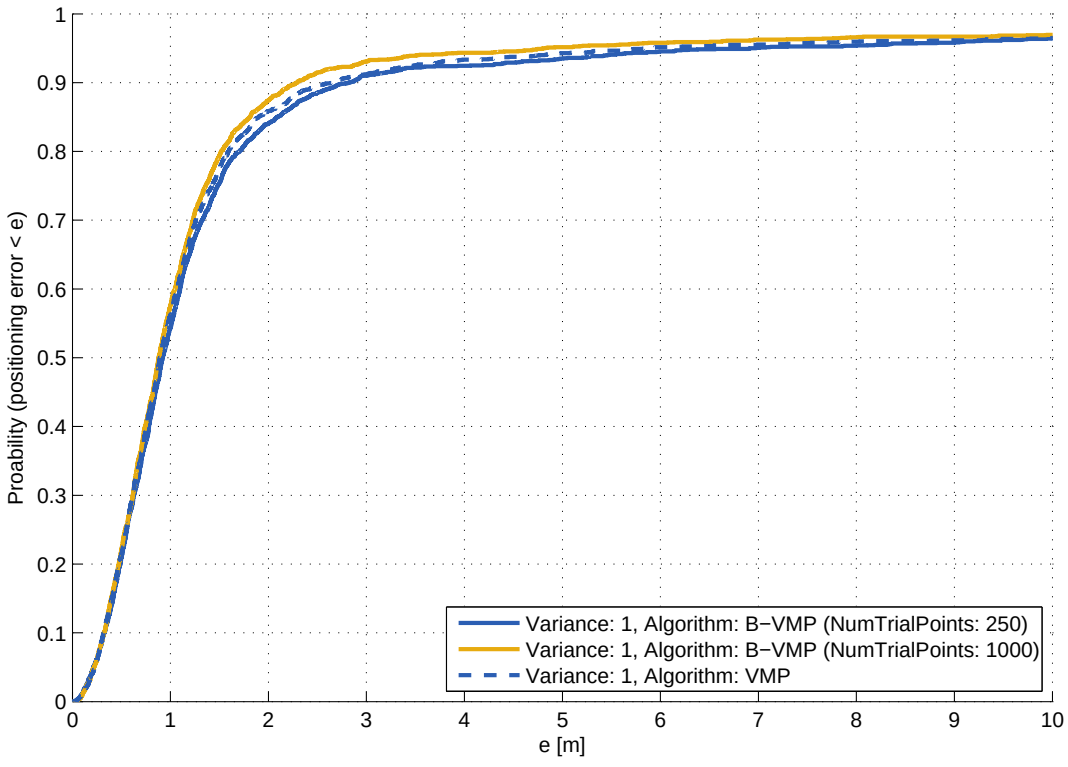

Figure 5.10: The blue lines are equal to chose from Figure 5.8(b). The orange line indicate the result of B-VMP algorithm re-run with `NumTrialPoints` setting at 1000 instead of 250 as is used for all the other plots.

5.2 WHERE2 DLR preliminary measurements

Within the WHERE2 project a couple of measurement campaigns have been carried out to evaluate the both the hardware and algorithms developed within the project. One of these measurement campaigns is termed "DLR preliminary" and resulted in the ICC paper shown in Appendix C. A part of this Master's project have been to evaluate the VMP algorithm on the WHERE2 measurements. This measurement campaign where conducted on the DLR premises in Germany (Deutsches Zentrum für Luft- und Raumfahrt). The measurement campaign included multiple scenarios but in this section only results from "Setup 2" will be considered. See Fig. 5 of Appendix C for details. The distance measurements used are obtained from the ZigBee nodes using RSSI. At the time when the paper was written the B-VMP algorithm was not implemented and hence results from this algorithm were not included in the paper.

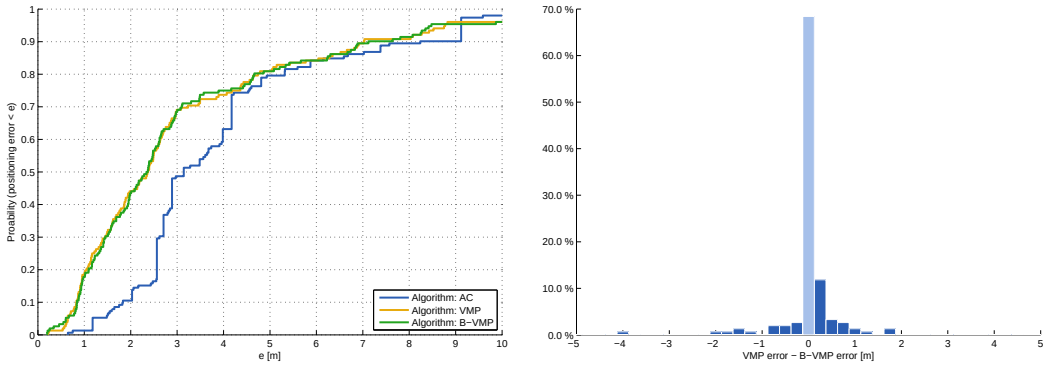

(a) CDF (b) Position error difference

Figure 5.11: Results from the DLR preliminary "Setup 2" scenario.

Figure 5.11 shows the result of the B-VMP algorithm evaluated on the DLR preliminary "Setup 2" scenario. As can be seen from 5.11(a) the results of B-VMP and VMP look similar. Figure 5.11(b) shows the differences of the position estimation errors. The result are that 55.9 % of the nodes are better located by B-VMP over VMP but 3.9 % is located worse than -1 m and only 2.6 % are better than 1 m.

This however does not mean that the benefits of the B-VMP algorithm is not present in the localization result. Figure 5.12 shows the position error per mobile node per iteration plot for the position request with index 26 (of 38). It can be seen that in this case the alternation between two sets of position estimates are eliminated in the B-VMP algorithm compared to VMP.

Looking at the CDF of Figure 5.11(a) it can be seen that only 45 % of the nodes are located within an error range of 2 m and 70 % within 3 m. This might seem somewhat inconvenient for and indoor localization application. However to evaluate the performance it is necessary to look at the input of the algorithms. Figure 5.13 shows the distance measurements for position request index 26. This is somewhat representative for the position request of scenario "Setup 2". From this figure it is clear that these scenarios both have low connectivity and that the distance measurement vary a lot. But as can be seen from the results in Figure 5.14 both algorithms find rather good position estimates anyway.

In this case the VMP algorithm performs a little better as it locates the mobile node with id 400 more accurately. However as the VMP algorithm alternates between two sets of position estimates (see Figure 5.12(a)) if the algorithm had been terminated one iteration before then this mobile node would have been located worse. Looking at the plots of $\tilde{p}_r(\boldsymbol{x}_r)$ in Figure 5.15 it can be seen that both algorithms have a bimodal $\tilde{p}_r(\boldsymbol{x}_r)$ for this node. The VMP algorithm chooses one of these modes whereas the B-VMP select both. This particular node shows the challenges of selecting the final position estimate of the B-VMP algorithm.

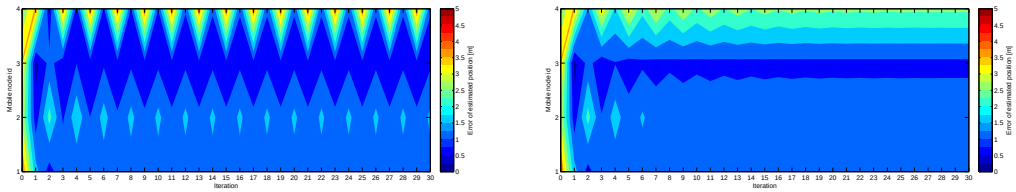

(a) VMP (b) B-VMP

Figure 5.12: Position estimate error for each mobile node for each iteration. For position request with index 26.

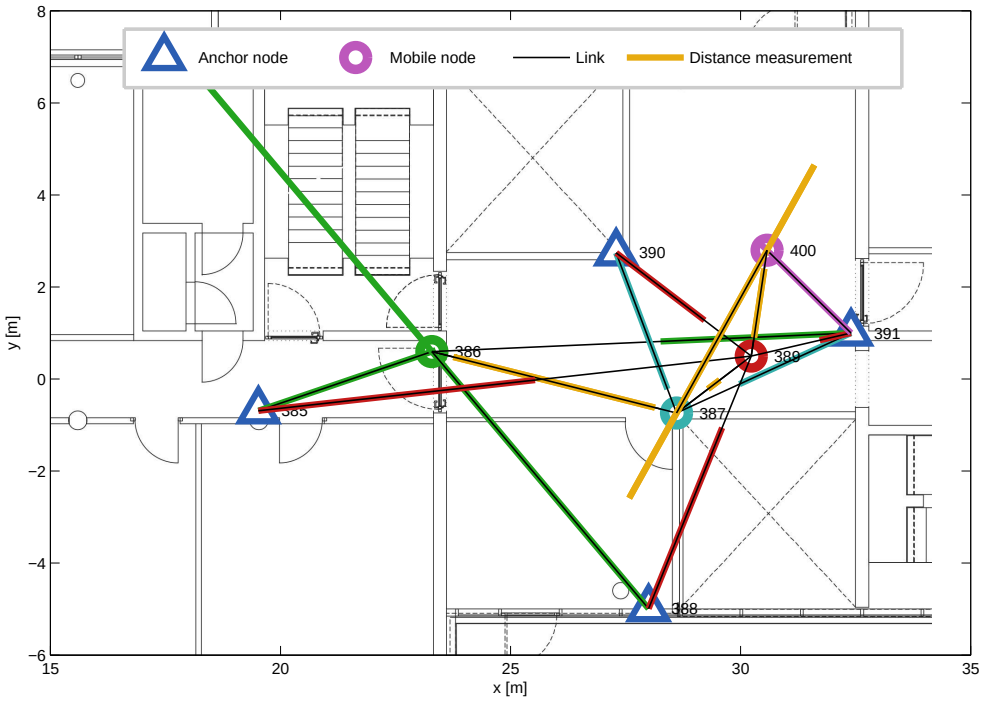

Figure 5.13: True positions and distance measurements for position request with index 26.

However the shown example is one of the better where the localization performance is resonable. For some position requests large erroneous distance measurements pushes the best position estimates way of course. As can be seen from Figure 5.11(a) close almost 20 % of the nodes are located with errors worse than 5 m. It is therefore interesting to see how these distance measurements from the real world look like. Figure 5.16 show a histogram of the distance measurement errors. Figure 5.17 shows a histogram of the distance measurement errors relative to their individual reported distance measurement

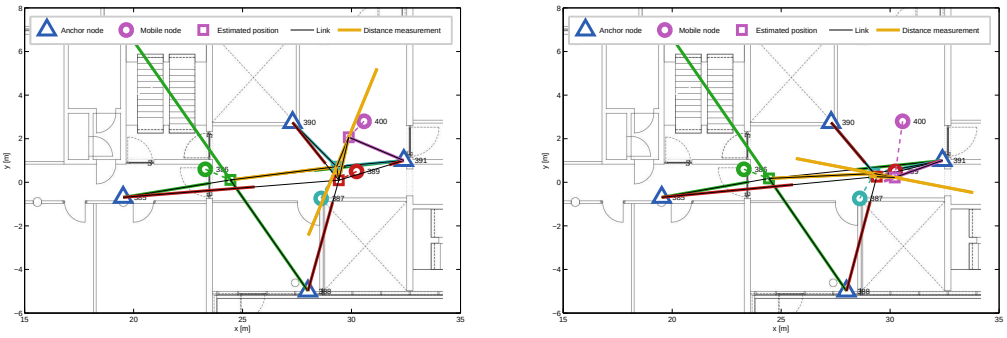

(a) VMP (b) B-VMP

Figure 5.14: Estimated positions obtained from the algorithms after 30 iterations. Distance measurements also shown. Position request index 26.

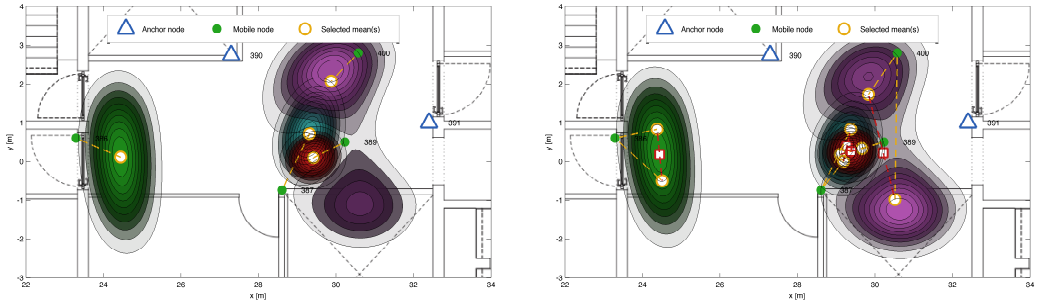

(a) (b)

Figure 5.15: Map of $\tilde{p}_r(\boldsymbol{x}_r)$ for each mobile node at last iteration (30). Position request index 26.

standard deviation $\sigma_{d_{r,t}}$. From these two plots it is clear the distance errors are not normally distributed. Furthermore is it clear the reported distance measurement standard deviation is not that reliable as there are many large outliners (of by multiple standard deviations). Actually 24.2 % of the distance measurements are of by more than 3 standard deviations.

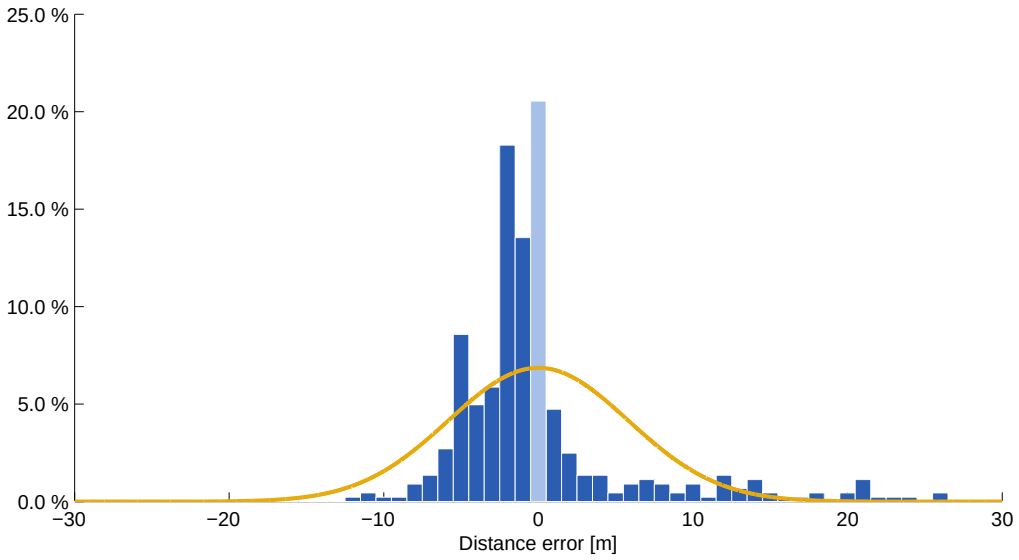

Figure 5.16: Histogram of all distance measurement errors. The yellow line shows a zero-mean scaled Gaussian for comparison.

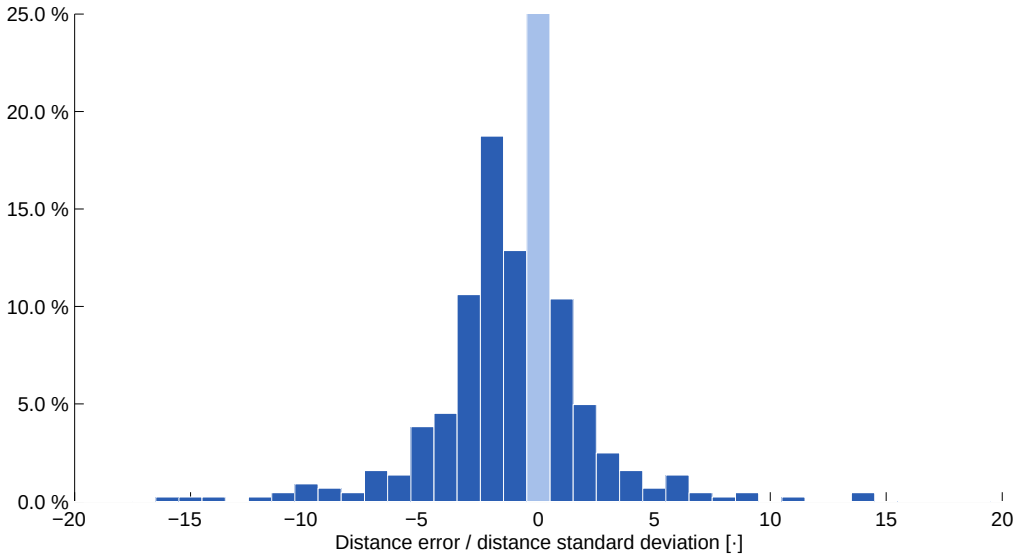

Figure 5.17: Histogram of distance measurements errors relative to their reported distance measurement error standard deviation.

6 Conclusion

Cooperative localization is clearly a good idea and it is obviously beneficial in otherwise low connectivity scenarios. However as presented in Chapter 4 distributed cooperative localization does involve a lot of practical challenges.

In this work the VMP algorithm by Pedersen et al. [1] is introduced and investigated. From both simulations and real world measurement data it is observed that the algorithm might end up alternating between two sets of position estimates and not converge to a single set. With this in mind a modified version is proposed that uses a bimodal approximation instead of the original unimodal approximation. This proposed algorithm is termed Bimodal Variational Message Passing (B-VMP).

Both algorithms are further investigated in pursuit of understanding their internal behaviour. A simple simulation scenario is defined and Monte Carlo simulations are performed. From these simulations it is concluded that the B-VMP algorithm does actually improve the position estimates compared to the original VMP algorithm.

It is also observed that both algorithms highly depends on an efficient and correct global minimization for the defined closed form KL-divergences. This minimization step might be quite computational demanding. Note that for the B-VMP algorithm a global minimum is searched for in a non-convex 7-dimensional space.

Besides the simulated scenarios both algorithms were as well tested on real world data from the WHERE2 project. It was observed that for this measurement scenario the algorithms perform equal to or better that alternative algorithms proposed within the WHERE2 project (see Appendix C).

From the work of this project it is clear that many more questions needs to be answered before this type of algorithm can be implemented in a real scenario.

6.1 Discussion

Before any further work is conducted a couple of things need to be considered. First of all it should be considered when and why distributed localization might be preferred over a centralized solution for some applications. A clearer understanding of the applications at hand will be favorable for any further work. Secondly it should be considered how to include any floor plan information in the algorithm. For applications with user interaction it is save to assume the floor plan is available in some digital format. Next it should be considered how potential multipath information from UWB signals can be exploited like in [6, 7, 8].

A Gradient of KL-divergence for VMP

For definition of the terms see Section 2.1. For the confluent hypergeometric function we use that [12]:

$$\frac{d\,\mathrm{M}(a,b,z)}{dz} = \frac{a}{b}\,\mathrm{M}(a+1,b+1,z) \tag{A.1}$$

With this the gradient can be derived as:

$$\frac{\partial\,\mathrm{KL}\left(q_r' \parallel \tilde{p}_r\right)}{\partial \dot{\sigma}_r^2} = \frac{1}{\tilde{\sigma}_r^2} - \frac{1}{\dot{\sigma}_r^2} \tag{A.2a}$$

$$+ \sum_{a \in \mathcal{N}_r \cap \mathcal{N}_A} \left[\frac{1}{\sigma_{d_{r,a}}^2} - \frac{d_{r,a}\sqrt{\frac{\pi}{2}}}{2\sigma_{d_{r,a}}^2} (\dot{\sigma}_r^2)^{-\frac{1}{2}}\,\mathrm{M}\left(-\frac{1}{2}, 1, -\frac{||\dot{\boldsymbol{\mu}}_r - \boldsymbol{\mu}_a||^2}{2\dot{\sigma}_r^2}\right) \right.$$

$$\left. + \frac{d_{r,a}\sqrt{\dot{\sigma}_r^2 \frac{\pi}{2}}}{\sigma_{d_{r,a}}^2} \frac{1}{2}\,\mathrm{M}\left(\frac{1}{2}, 2, -\frac{||\dot{\boldsymbol{\mu}}_r - \boldsymbol{\mu}_a||^2}{2\dot{\sigma}_r^2}\right) \frac{||\dot{\boldsymbol{\mu}}_r - \boldsymbol{\mu}_a||^2}{2(\dot{\sigma}_r^2)^2} \right] \tag{A.2b}$$

$$+ \sum_{m \in \mathcal{N}_r \cap \mathcal{N}_M} \left[\frac{1}{\sigma_{d_{r,m}}^2} - \frac{d_{r,m}\sqrt{\frac{\pi}{2}}}{2\sigma_{d_{r,m}}^2} (\dot{\sigma}_r^2 + \hat{\sigma}_m^2)^{-\frac{1}{2}}\,\mathrm{M}\left(-\frac{1}{2}, 1, -\frac{||\dot{\boldsymbol{\mu}}_r - \hat{\boldsymbol{\mu}}_m||^2}{2(\dot{\sigma}_r^2 + \hat{\sigma}_m^2)}\right) \right.$$

$$\left. + \frac{d_{r,m}\sqrt{(\dot{\sigma}_r^2 + \hat{\sigma}_m^2)\frac{\pi}{2}}}{\sigma_{d_{r,m}}^2} \frac{1}{2}\,\mathrm{M}\left(\frac{1}{2}, 2, -\frac{||\dot{\boldsymbol{\mu}}_r - \hat{\boldsymbol{\mu}}_m||^2}{2(\dot{\sigma}_r^2 + \hat{\sigma}_m^2)}\right) \frac{||\dot{\boldsymbol{\mu}}_r - \hat{\boldsymbol{\mu}}_m||^2}{2(\dot{\sigma}_r^2 + \hat{\sigma}_m^2)^2} \right] \tag{A.2c}$$

$$\frac{\partial\,\mathrm{KL}\left(q_r' \parallel \tilde{p}_r\right)}{\partial \dot{\mu}_{r,i}} = \frac{\dot{\mu}_{r,i} - \tilde{\mu}_{r,i}}{\tilde{\sigma}_r^2} \tag{A.3a}$$

$$+ \sum_{a \in \mathcal{N}_r \cap \mathcal{N}_A} \frac{\dot{\mu}_{r,i} - \mu_{a,i}}{\sigma_{d_{r,a}}^2} + \frac{d_{r,a}\sqrt{\dot{\sigma}_r^2 \frac{\pi}{2}}}{\sigma_{d_{r,a}}^2} \frac{1}{2}\,\mathrm{M}\left(\frac{1}{2}, 2, -\frac{||\dot{\boldsymbol{\mu}}_r - \boldsymbol{\mu}_a||^2}{2\dot{\sigma}_r^2}\right) \frac{\dot{\mu}_{r,i} - \mu_{a,i}}{2\dot{\sigma}_r^2} \tag{A.3b}$$

$$+ \sum_{m \in \mathcal{N}_r \cap \mathcal{N}_M} \frac{\dot{\mu}_{r,i} - \hat{\mu}_{m,i}}{\sigma_{d_{r,m}}^2} + \frac{d_{r,m}\sqrt{(\dot{\sigma}_r^2 + \hat{\sigma}_m^2)\frac{\pi}{2}}}{\sigma_{d_{r,m}}^2} \frac{1}{2}\,\mathrm{M}\left(\frac{1}{2}, 2, -\frac{||\dot{\boldsymbol{\mu}}_r - \hat{\boldsymbol{\mu}}_m||^2}{2(\dot{\sigma}_r^2 + \hat{\sigma}_m^2)}\right) \frac{\dot{\mu}_{r,i} - \hat{\mu}_{m,i}}{2(\dot{\sigma}_r^2 + \hat{\sigma}_m^2)} \tag{A.3c}$$

where $i \in \{1, 2\}$ is the vector component index.

B Gradient of KL-divergence for B-VMP

For definition of the terms see Section 3.1. As the closed form expression of the KL-divergence for the bimodal case consists of the same building blocks as for the unimodal case the gradients will as well consist of the same blocks (although scaled by appertaining weights). See Appendix A for details on the contributions from the neighbouring nodes. The gradient for $\dot{w}_{r,1}$ for these parts is trivial to derive. Only the part from (3.4a) (i.e. eq. (3.6)) is significantly different and will be derived here.

Since this is only to be used for the bimodal case we will rewrite (3.4a) using that $K = 2$, $\dot{w}_{r,2} = (1 - \dot{w}_{r,1})$, and that $\mathrm{KL}(f_a \parallel f_a) = 0$. For clarity we first define q_k and $\tilde{q}$.

$$q_k(\boldsymbol{x}_r) = \mathcal{N}(\boldsymbol{x}_r \mid \dot{\boldsymbol{\mu}}_{r,k}, \dot{\sigma}^2_{r,k}) \tag{B.1}$$

$$\tilde{q}(\boldsymbol{x}_r) = \mathcal{N}(\boldsymbol{x}_r \mid \tilde{\boldsymbol{\mu}}_r, \tilde{\sigma}^2_r) \tag{B.2}$$

And (3.4a) then becomes:

$$\mathrm{KL}\left(q'_r \parallel \tilde{q}\right) \approx \sum_{k=1}^{K} \dot{w}_{r,k} \ln \frac{\sum_{l=1}^{K} \dot{w}_{r,l} \exp\left(-\mathrm{KL}\left(q_k \parallel q_l\right)\right)}{\exp\left(-\mathrm{KL}\left(q_k \parallel \tilde{q}\right)\right)} \tag{B.3}$$

$$\begin{aligned} &= \dot{w}_{r,1}\Big(\ln\Big(\dot{w}_{r,1} + (1 - \dot{w}_{r,1}) \exp\left(-\mathrm{KL}\left(q_1 \parallel q_2\right)\right)\Big) + \mathrm{KL}\left(q_1 \parallel \tilde{q}\right)\Big) \\ &\quad + (1 - \dot{w}_{r,1})\Big(\ln\Big((1 - \dot{w}_{r,1}) + \dot{w}_{r,1} \exp\left(-\mathrm{KL}\left(q_2 \parallel q_1\right)\right)\Big) + \mathrm{KL}\left(q_2 \parallel \tilde{q}\right)\Big) \end{aligned} \tag{B.4}$$

From (B.4) we can derive the gradient for this part:

$$\begin{aligned} \frac{\partial\, \mathrm{KL}\left(q'_r \parallel \tilde{q}\right)}{\partial \dot{w}_{r,1}} &= \mathrm{KL}\left(q_1 \parallel \tilde{q}\right) - \mathrm{KL}\left(q_2 \parallel \tilde{q}\right) + \ln\Big(\dot{w}_{r,1} + (1 - \dot{w}_{r,1}) \exp\left(-\mathrm{KL}\left(q_1 \parallel q_2\right)\right)\Big) \\ &\quad + \frac{\dot{w}_{r,1}\Big(1 - \exp\left(-\mathrm{KL}\left(q_1 \parallel q_2\right)\right)\Big)}{\dot{w}_{r,1} + (1 - \dot{w}_{r,1}) \exp\left(-\mathrm{KL}\left(q_1 \parallel q_2\right)\right)} \\ &\quad + \frac{-1 + \exp\left(-\mathrm{KL}\left(q_2 \parallel q_1\right)\right)}{(1 - \dot{w}_{r,1}) + \dot{w}_{r,1} \exp\left(-\mathrm{KL}\left(q_2 \parallel q_1\right)\right)} \\ &\quad - \ln\Big((1 - \dot{w}_{r,1}) + \dot{w}_{r,1} \exp\left(-\mathrm{KL}\left(q_2 \parallel q_1\right)\right)\Big) \\ &\quad - \frac{\dot{w}_{r,1}\left(-1 + \exp\left(-\mathrm{KL}\left(q_2 \parallel q_1\right)\right)\right)}{(1 - \dot{w}_{r,1}) + \dot{w}_{r,1} \exp\left(-\mathrm{KL}\left(q_2 \parallel q_1\right)\right)} \end{aligned} \tag{B.5}$$

and for simplicity we introduce $\bar{k} \in \{1,2\} \setminus k$:

$$\frac{\partial \operatorname{KL}\left(q'_r \parallel \tilde{q}\right)}{\partial \dot{\sigma}^2_{r,k}} = \dot{w}_{r,k}\left(\frac{1}{\tilde{\sigma}^2_r} + \frac{1}{\dot{w}_{r,k}} + \frac{\dot{w}_{r,\bar{k}} \exp\left(-\operatorname{KL}\left(q_k \parallel q_{\bar{k}}\right)\right)}{\dot{w}_{r,k} + \dot{w}_{r,\bar{k}} \exp\left(-\operatorname{KL}\left(q_k \parallel q_{\bar{k}}\right)\right)}\left(-\frac{1}{\dot{\sigma}^2_{r,\bar{k}}} + \frac{1}{\dot{\sigma}^2_{r,k}}\right)\right) + \dot{w}_{r,\bar{k}}\left(\frac{\dot{w}_{r,k} \exp\left(-\operatorname{KL}\left(q_{\bar{k}} \parallel q_k\right)\right)}{\dot{w}_{r,\bar{k}} + \dot{w}_{r,k} \exp\left(-\operatorname{KL}\left(q_{\bar{k}} \parallel q_k\right)\right)}\left(\frac{\dot{\sigma}^2_{r,\bar{k}}}{(\dot{\sigma}^2_{r,k})^2} + \frac{\left|\left|\dot{\boldsymbol{\mu}}_{r,\bar{k}} - \dot{\boldsymbol{\mu}}_{r,k}\right|\right|^2}{(\dot{\sigma}^2_{r,k})^2} - \frac{1}{\dot{\sigma}^2_{r,k}}\right)\right) \tag{B.6}$$

$$\frac{\partial \operatorname{KL}\left(q'_r \parallel \tilde{q}\right)}{\partial \dot{\mu}_{r,k,i}} = \dot{w}_{r,k}\left(\frac{\dot{\mu}_{r,k,i} - \tilde{\mu}_{r,i}}{\tilde{\sigma}^2_r} + \frac{\dot{w}_{r,\bar{k}} \exp\left(-\operatorname{KL}\left(q_k \parallel q_{\bar{k}}\right)\right)}{\dot{w}_{r,k} + \dot{w}_{r,\bar{k}} \exp\left(-\operatorname{KL}\left(q_k \parallel q_{\bar{k}}\right)\right)}\left(\frac{\dot{\mu}_{r,k,i} - \dot{\mu}_{r,\bar{k},i}}{\dot{\sigma}^2_{r,\bar{k}}}\right)\right) + \dot{w}_{r,\bar{k}}\left(\frac{\dot{w}_{r,k} \exp\left(-\operatorname{KL}\left(q_{\bar{k}} \parallel q_k\right)\right)}{\dot{w}_{r,\bar{k}} + \dot{w}_{r,k} \exp\left(-\operatorname{KL}\left(q_{\bar{k}} \parallel q_k\right)\right)}\left(\frac{\dot{\mu}_{r,\bar{k},i} - \dot{\mu}_{r,k,i}}{\dot{\sigma}^2_{r,k}}\right)\right) \tag{B.7}$$

where $i \in \{1,2\}$ is the vector component index.

C ICC 2013 Paper

Cooperative and Heterogeneous Indoor Localization Experiments

B. Denis[♯], R. Raulefs[†], B.H. Fleury[♮], N. Amiot[¶], L. de Celis[‡], J. Dominguez[‡], M.B. Koldsgaard[♮], M. Laaraiedh[¶], H. Noureddine[§], E. Staudinger[†], G. Steinboeck[♮]
[†]German Aerospace Center - DLR, Wessling, Germany
[‡]Acorde Technologies S.A, Control Applications Development, Santander, España
[♯]CEA-Leti Minatec Campus, System Integration Dept, Grenoble, France
[♮]Aalborg University, Electronic Systems Dept, Aalborg, Denmark
[§]Mitsubishi Electric R&D Centre Europe, Rennes, France
[¶]Université Rennes 1 - IETR, CNRS UMR6164, Rennes, France
E-mails: benoit.denis@cea.fr

***Abstract*—In this paper we present the results of real-life localization experiments performed in an unprecedented cooperative and heterogeneous wireless context. These measurements are based on ZigBee and orthogonal frequency division multiplexing (OFDM) devices, respectively endowed with received signal strength indicator (RSSI) and round trip delay (RTD) estimation capabilities. More particularly we emulate a multi-standard terminal, moving in a typical indoor environment, while communicating with fixed OFDM-based femto-base stations (Femto-BSs) and with other mobiles or fixed anchor nodes (through peer-to-peer links) forming a wireless sensor network (WSN). We introduce the measurement functionalities and metrics, the scenario and set-up, providing realistic connectivity and obstruction conditions. Out of the experimental data, preliminary positioning results based on cooperative and geometric algorithms are finally discussed, showing benefits through mobile-to-mobile cooperation, selective hybrid data fusion and detection of unreliable nodes.**

I. Introduction

Most of our usual environments comprise heterogeneous wireless resources, such as WiFi access points (APs), Long Term Evolution (LTE) femto base stations (Femto-BSs) and wireless sensor networks (WSNs). These environments are also densely crowded by multi-standard mobile terminals (MTs) cooperating directly over short or medium ranges. In such environments, the radiolocation capability has been clearly identified as a key feature in order to enhance the connectivity experience (i.e. providing ubiquitous wireless access, extended context-dependent service coverage or increased data rates through e.g., vertical handover) and to provide indoor navigation or even beyond, new context-based services [1].

Algorithmic works reported in the recent literature have been focusing on decentralized iterative positioning (e.g. [2], [3], [4]) on the one hand, and cooperative links selection (e.g. [5], [6]) on the other hand, but the localization performance has been uniquely assessed through simulations so far. The latter evaluations can obviously not account for complex phenomena inherent to jointly cooperative and heterogeneous contexts, such as space-time correlations (inter- or intra-radio) between the different involved radio access technologies (RATs), the conjunction of harmful sparse connectivity and poor geometric dilution of precision (GDoP) conditions, or erratic radio obstructions experienced along the MT trajectory (e.g. due to small pieces of metallic furniture [7]), etc.

In this paper, we describe a real-life localization-oriented measurement campaign realized in a cooperative and heterogeneous wireless indoor context, based on ZigBee and OFDM devices. The ZigBee devices are enabled with received signal strength (RSS) measurement capabilities. The OFDM setup allows for round trip delay (RTD) estimation. Applying decentralized iterative message-passing and non-cooperative geometric positioning to the extracted experimental data, we show the clear benefits observed through selective peer-to-peer (P2P) short-range cooperation and multi-RAT hybrid data fusion, considering different path loss models to represent such harsh indoor scenarios in more detail.

The paper is structured as follows. In Section II, we recall the main characteristics of the involved OFDM and ZigBee radio devices. Section III describes our experimental setup, along with the covered indoor scenarios. Section IV subsequently reports positioning results obtained through decentralized cooperative message-passing and geometric algorithms based on the measurement data.

II. Available Radio Access Technologies and Location-Dependent Metrics

A. RTD-Enabled OFDM Devices

In the context of the WHERE2 project [1], we developed a flexible test-bed that allows for P2P ranging based on analogue amplify RTD. Fig. 1 shows the test-bed [8] embedded in the multi-standard MT. The analogue amplify RTD determines, based on the fixed processing delay in the return node, the distance similarly to the time of arrival (ToA) method. The test-bed consists of two parts, a master node and a slave node. The master node transmits an OFDM modulated signal to the slave node. The slave node returns this signal amplified. The master node receives the signal from the slave node and estimates the RTD to determine the distance. This approach

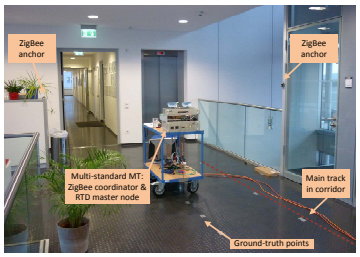

Fig. 1. Photograph of the multi-standard MT mounted on a trolley in the small open space area.

simplifies the synchronization between both nodes. The key system parameters are a sampling rate of 120 MHz with a subcarrier spacing of 14.65 kHz. Only the inner 512 subcarriers are active, which results in an effective bandwidth of 36.62 MHz. The center frequency of the master-to-slave link is 5.5 GHz and the reverse link is 5.7 GHz. The transmit power was limited to 21 dBm.

In the setup, RTD estimation is based on a correlation receiver with interpolation. Thus, it is possible to obtain fractional sample delays which leads to high ranging accuracy. The structure of the OFDM modulated signals is similar to that used in 3GPP-LTE. This allows for future investigations of flexible allocation schemes of subcarriers to steer the ranging performance depending on the requirements. Fig. 2 shows the ranging performance versus distance for different propagation conditions in the investigated indoor environment. We distinguish between three constellations characterized by the position of the MT: corridor (LoS1), open area close to the right end of the corridor (LoS2), and open area (NLoS), see the dotted-line trajectory on Fig. 4. As indicated by the used acronyms, the two former constellations correspond to line of sight (LoS) transmission, while the latter is a non-line of sight (NLoS) condition. As expected we can observe in Fig. 2 a performance degradation as the distance between the RTD anchor and the MT increases. The observed larger distance errors at the end of the corridor and in the open area are caused by more severe multipath propagation.

B. RSS-Enabled ZigBee Devices

The radio transceiver is based on the CC2431 Texas Instruments. This chip is a solution for IEEE 802.15.4 and ZigBee applications. Regarding the RSSI measurement the more relevant CC2431 radio parameters are the operation frequency of 2.4 GHz with a bandwidth of 5 MHz, a TX power of 0 dBm and a RX sensitive of -92 dBm.

We use the one-slope pathloss model [9] to infer on the ranges from the experimentally obtained RSSI values of the ZigBee nodes. For the range estimation we follow the method described in [10]. The parameters of the one slope model are the reference power P_0, obtained at reference distance $d_0 = 1$ m, and the path loss exponent n_p, which characterizes the power decay versus distance. The deviations of experimental

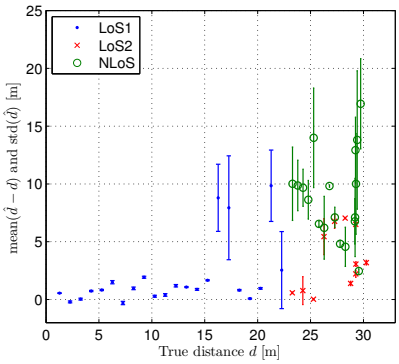

Fig. 2. RTD ranging performance versus distance obtained with the used correlator in the investigated indoor environment. Different propagation conditions are considered: LoS1 (in the long corridor), LoS2 (after the corridor in the open space), and NLoS (in the open space).

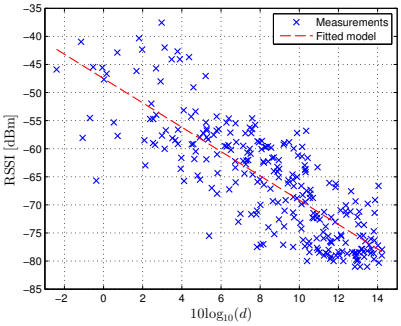

Fig. 3. Cluster plot of the experimental RSSI values obtained in Setup 1 (see Section III-A) versus distance together with the pathloss model using the "global" settings reported in Tab. I.

RSSI values from the pathloss model are commonly modeled as realizations of a zero-mean Gaussian random variable with variance σ^2_{sh}. The pathloss parameters are environment dependent and are determined empirically from a set of calibration measurements. For the presented results we estimated the model parameters from the measurement setup described in Section III-A using a Least Squares (LS) estimator. We report in Tab. I the estimated parameters together with parameter values from the data sheet of the ZigBee transceiver of a non-specified scenario [11] and label them "global" and "data sheet", respectively. The measured RSSI values and the fitted model are shown in Fig. 3.

III. Measurement Setups and Scenarios

The measurement campaign is part of an integration and validation step between ZigBee nodes and a RTD test-bed developed in the frame of the WHERE2 project. Measurement results are provided within the WHERE2 project to enable

TABLE I
PATHLOSS MODEL PARAMETERS.

	P_0 [dBm]	n_p	σ_{sh}[dB]
data sheet	-42	3	5.0
global	-47	2	5.8

algorithm verification and benchmarking for interested partners. The measurement data is available on the WHERE2 website [1].

A. Setup 1: Nominal Cooperative and Heterogeneous Scenario

In this setup we aim to cover the whole measurement area with the used ZigBee nodes. This allows verification of cooperative / non-cooperative positioning algorithms and the extraction of shadowing maps. Fig. 4 shows a simplified floorplan with the positions of the ZigBee nodes and the RTD slave anchor and Fig. 1 depicts a photograph of the measurement setup. The RTD slave node is located at the end of the corridor, to allow LoS ranging for the majority of ground-truth points (GTPs). The ZigBee anchors are distributed in a way to satisfy the limited communication range as well as to reduce the GDoP along the main track. Our multi-standard MT is comprised of the RTD master node and one ZigBee coordinator mounted on a trolley. Measurements are performed at stationary positions for approximately 100 s each. GTPs along the corridor are separated by 1 m and GTPs perpendicular to the corridor track or parallel to the corridor track are separated by 0.5 m. The provided GTPs have an accuracy better than 2 cm.

Furthermore, we chose one ZigBee node mounted on a tripod as mobile node, crossing the main track in the corridor, see the green dashed line in Fig. 4. The multistandard MT moves from the RTD slave node along the corridor, whilst in parallel, this specific mobile node walks along its own GTP-track. Thus, this additional mobile node can either be exploited as moving anchor node or as cooperative node with estimated position.

B. Setup 2: Impact of Peer-to-Peer Connectivity

The second measurement setup aims for a further evaluation of cooperation through peer-to-peer (P2P) links. All ZigBee anchors are located in a small open space area, see Fig. 5. Thus, we have an environment with multiple P2P links and a generally overdetermined positioning system. This helps evaluate the potential of more sophisticated cooperative positioning algorithms, e.g., GDoP reduction and link selection. The measurement procedure is similar to that used for Setup 1, but we start in the middle of the corridor only. This ensures a fully connected network in which the ZigBee coordinator on the MT has valid ranging links to all anchors.

IV. TESTED ALGORITHMS AND PRELIMINARY RESULTS

In this section, we apply selected positioning algorithms developed in the frame of WHERE2 onto experimental ranges

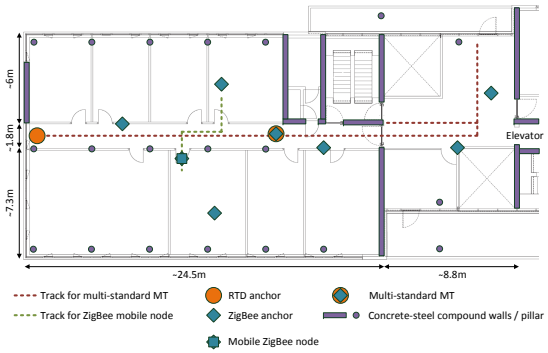

Fig. 4. Cooperative and heterogeneous Setup 1: Back-and-forth trajectory of a multi-standard OFDM-RTD/ZigBee MT in a corridor and small open area with 7 ZigBee anchors and 1 RTD anchor.

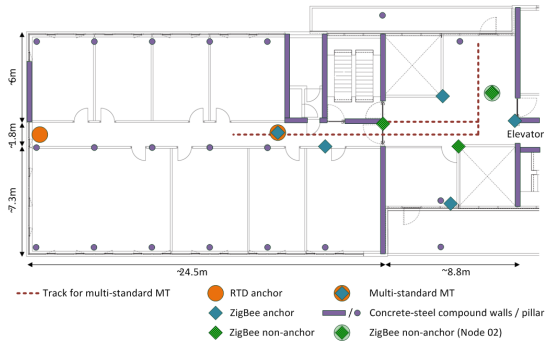

Fig. 5. Cooperative and heterogeneous Setup 2: Identical multi-standard MT track but with locally higher short-range peer-to-peer connectivity in the small open area.

derived from RTD and RSSI measurements (from both setups 1 and 2). In the latter case, RSSI-based range information is derived using estimators from [10], while using the in-site path loss model parameters discussed in Section II-B.

A. Non-cooperative Positioning

The non-cooperative RGPA algorithm described in [12], which is based on geometric representation of the location dependent metrics (LDPs), is applied to experimental data from measurement Setup 1. We consider all the RSSI values measured between the fixed ZigBee anchors and the ZigBee coordinator of the multi-standard MT. Fig. 6 shows the cumulative distribution function (CDF) of estimated location errors, with and without incorporating the OFDM RTD measurement on top of the ZigBee RSSI measurements, illustrating the clear benefits that can be achieved through hybrid data fusion in comparison with homogeneous WSN localization. Fig. 6 also presents a comparison with a non-cooperative maximum likelihood (ML) positioning algorithm, initialized with a random guess drawn on the scene of interest. The comparison

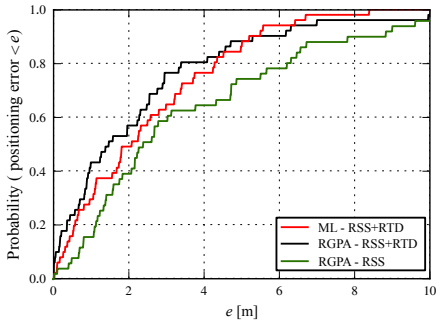

Fig. 6. CDF of positioning errors for the RGPA and randomly initialized ML positioning algorithms, with and without incorporating the OFDM RTD measurement on top of ZigBee RSSI measurements.

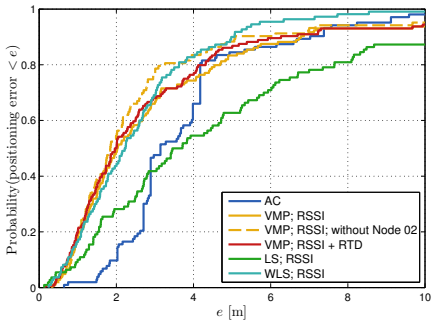

Fig. 7. CDF of positioning errors for the AC, VMP, LS and WLS algorithms. Furthermore VMP is shown excluding unreliable "Node 02" (dashed orange) and including RTD measurements (red).

reveals that the geometric algorithm slightly outperforms the ML solution in the small and medium location error regimes at the benefit of much lower computational complexity, while suffering from performance degradation in the order of 1 m only in the worst case location error regime caused by severe measurement outliers (i.e. beyond a location error of 4 m at 90% of the CDF), where the ML error would be anyway larger than practical target thresholds in most indoor applications.

B. Cooperative Positioning

In these investigations we compare the cooperative and decentralized variational message-passing (VMP) solution described in [2], cooperative centralized least squares (LS) and weighted least squares (WLS) algorithms [13] and a non-cooperative decentralized anchor centroid (AC) solution [14]. The latter is used as initialization in the VMP algorithm. The LS and WLS algorithms obtain initial starting positions from a semi definite programming (SDP) algorithm [15]. For all algorithms we consider the data from the fixed OFDM RTD anchor, 4 fixed ZigBee anchors, 3 ZigBee non-anchor nodes (with unknown positions) and the multi-standard mobile trolley in Setup 2, see Fig. 5. We estimate the positions of the non-anchor nodes and the mobile trolley with the above positioning algorithms and evaluate their performance in terms of positioning accuracy. Fig. 7 shows the CDFs of the positioning errors for the different algorithms.

The VMP algorithm uses link-specific standard deviations in the distance-error model. These standard deviations are computed from distances estimated from multiple RSSI readings. For the RTD measurement we distinguish between LoS and NLoS conditions and set the standard deviation to 0.25 m and 1.5 m, respectively. For the WLS algorithm we select the weights as $w_{i,j} = 1/\hat{d}_{i,j}^2$ where $\hat{d}_{i,j}$ is the estimated distance between nodes i and j. The AC algorithm solely relies on the positions of anchors to which a link is available.

We observe that all algorithms perform better than the AC method, except the LS for position errors larger than 3 m. For position errors larger than 4 m all algorithms are above 80% of the CDF and perform similar to the AC method. Only the WLS seems to perform slightly better. We observe further that VMP and WLS seem to perform equally well for practical error ranges smaller than 3 m.

For the heterogeneous case (inclusion of RTD measurements) we observe only a small benefit for position errors larger than 3.8 m in the VMP algorithm. The gain in Setup 1 is more pronounced as shown in Fig. 6. This is maybe due to the fact that in Setup 1 LoS conditions prevail and that generally the distances are larger, as such the expected distance errors obtained from the RSSI measurements are larger, which leads to a more significant improvement from the RTD measurements.

We observed that the RSSI readings of node 02 (see Fig. 5) exhibit much larger fluctuations compared to the readings of other nodes. By comparison of the CDFs for the VMP with and without node 02 in Fig. 7 we see that for positioning errors larger than 2 m the results without this node seem to be improved. More specifically an error gain of 1 m is obtained at 80% of the CDF. Thus, node 02 is unreliable and its readings should be discarded. This example illustrates the benefits of detecting and incorporating solely the most reliable cooperative nodes. This problem of link selection is one of the ongoing topics within WHERE2 (e.g. based on link quality, GDoP, location error CRLB, or a combination of the previous criteria [5], [6]).

C. Sensitivity to a priori *Path Loss Models and Parameters*

We investigate the sensitivity of the positioning errors of the RGPA, VMP, and WLS algorithms for different path loss model settings in the prior RSSI-based ranging step. The CDFs of position errors are shown for each algorithm using two different path loss model settings in Fig. 8. The results for VMP and WLS are obtained for Setup 2 using path loss model settings "global" and "data sheet". The results for RGPA are obtained for Setup 1 using the "global" path loss model, and using an individual path loss model for each ZigBee node termed "node specific" in the figure. The "node specific" set of path loss models (dashed blue curve) provides only a slight

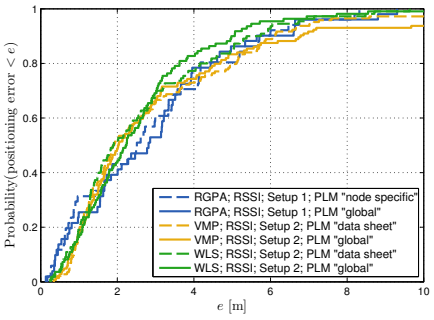

Fig. 8. CDF of positioning errors for RGPA, VMP, and WLS using the different path loss model settings reported in Tab. I.

improvement over the fixed "global" path loss model (blue curve) in the practical error range (up to 3 m) for indoor localization. Hence from these preliminary results no clear benefit of using individually tailored path loss model settings is seen. The CDFs of VMP and WLS (orange vs. dashed orange and green vs. dashed green) show that both algorithms seem to be rather insensitive to the selected path loss model. This apparent insensitivity is likely caused by the relatively large variance of the RSSI measurements. The large variance of the RSSI measurements could also explain why the RGPA results do not improve much when the "node specific" path loss models are utilized, even though such node specific in-site self-learning have been shown valuable [7].

V. Conclusion

In this paper we presented a heterogeneous and cooperative positioning test-bed. This test-bed combines a single OFDM-based radio device using time-based distance measurements together with multiple ZigBee nodes that rely on the received signal strength indicator to estimate relative ranges. The measured data was collected and post-processed by different positioning algorithms, including a cooperative variational message-passing solution, and a non-cooperative geometric algorithm, both developed in the frame of the WHERE2 project. Cooperative positioning in indoor environments must classically cope with fast changing conditions, in terms of individual nodes mobility and problem geometry. In our investigations, the ranging devices also created additional outliers of range estimates (e.g. one node being even totally unreliable), which are representative of real-life operating conditions. This causes new challenges for the established algorithms that were investigated and compared. A few insights have thus been disclosed in favor of context-aware data fusion (e.g. depending on LOS/NLOS condition) and selective cooperation through links weighting or nodes censoring. Furthermore, even if most algorithms are parametric (in the sense that they would require a priori models of the expected measurement data), the proposed performance assessment tends to show that they are rather insensitive to using either values from the literature or refined models based on in-site measurements, at least in practical indoor localization error regimes.

The previous results, which are preliminary but not yet definitive, will be completed and further analyzed in the final version of the paper. The new inputs could concern the application of other message passing algorithms such as Non Parametric Belief Propagation (NBP), as well as the mitigation of unreliable cooperative nodes or poor hybrid measurements.

Acknowledgment

This work was performed in the framework of the WHERE2 (ICT-248894) project, which is partly funded by the European Commission.

References

[1] http://www.ict-where2.eu/.

[2] C. Pedersen, T. Pedersen, and B. H. Fleury. A variational message passing algorithm for sensor self-localization in wireless networks. In *IEEE International Symposium on Information Theory (ISIT 2011)*, pages 2158 –2162, Saint-Petersburg, Russia, August 2011.

[3] V. Savic, H. Wymeersch, F. Penna, and S. Zazo. Optimized edge appearance probability for cooperative localization based on tree-reweighted nonparametric belief propagation. In *IEEE International Conference on Acoustics, Speech and Signal Processing (ICASSP 2011)*, pages 3028–3031, Prague, Czech Republic, May 2011.

[4] H. Noureddine, N. Gresset, D. Castelain, and R. Pyndiah. A New Variant of Nonparametric Belief Propagation for Self-Localization. In *Proc. IEEE Int. Conf. on Telecommunications*, ICT'010, pages 822–827, April 2010.

[5] S. Hadzic, J. Bastos, and J. Rodriguez. Reference node selection for cooperative positioning using coalition formation games. In *Positioning Navigation and Communication (WPNC), 2012 9th Workshop on*, pages 105 –108, march 2012.

[6] S. Zirari and B. Denis. Comparison of links selection criteria for mobile terminal positioning in cooperative heterogeneous networks. In *Proceedings of Conference of Software, Telecommunications and Computer Networks (SoftCOM 2012)*, Split, Croatia, September 2012.

[7] B. Uguen, M. Laaraiedh, B. Denis, J. Keignart, J. Stephan, and Y. Lostanlen. Extraction and characterization of location-dependent uwb radio features with practical implications for indoor positioning. *European Wireless, 2012. EW. 18th European Wireless Conference*, pages 1 –10, april 2012.

[8] E. Staudinger and S. Sand. Generic real-time round-trip-delay test-bed for cooperative positioning. In *Proc. of 9th Workshop on Positioning Navigation and Communication*, pages 94 – 99, Dresden, Germany, March 2012.

[9] E. Damosso, editor. *Digital mobile radio towards future generation systems: Cost 231 Final Report*. European Commission, Bruxelles, Belgium, 1999.

[10] M. Laaraiedh, S. Avrillon, and B. Uguen. Enhancing positioning accuracy through direct position estimators based on hybrid rss data fusion. In *Vehicular Technology Conference, 2009. VTC Spring 2009. IEEE 69th*, april 2009.

[11] Texas Instrument. System-on-chip for 2.4 ghz zigbee. Technical report, Chipcon, Oct. 2005.

[12] N. Amiot, M. Laaraiedh, and B. Uguen. Evaluation of a geometric positioning algorithm for hybrid wireless networks. In *Proceedings of Conference of Software, Telecommunications and Computer Networks (SoftCOM 2012)*, Split, Croatia, September 2012.

[13] G. Destino and G.T.F. De Abreu. Weighing strategy for network localization under scarce ranging information. *IEEE Trans. Wireless Commun.*, 8(7):3668–3678, July 2009.

[14] N. Bulusu, J. Heidemann, and D. Estrin. GPS-less Low-Cost Outdoor Localization for Very Small Devices. *Personal Communications, IEEE*, 7(5):28–34, October 2000.

[15] P. Biswas, T. Lian, T. Wang, and Y. Ye. Semidefinite Programming Based Algorithms for Sensor Network Localization. *ACM Trans. Sen. Netw.*, 2(2):188–220, May 2006.

References

[1] C. Pedersen, T. Pedersen, and B. H. Fleury, "A variational message passing algorithm for sensor self-localization in wireless networks," in *Proceedings of the 2011 IEEE International Symposium on Information Theory*, Aug. 2011, pp. 2158–2162.

[2] WHERE2 project website. [Online]. Available: http://www.ict-where2.eu

[3] G. Sun, J. Chen, W. Guo, and K. Liu, "Signal processing techniques in network-aided positioning: a survey of state-of-the-art positioning designs," *Signal Processing Magazine, IEEE*, vol. 22, no. 4, pp. 12–23, 2005.

[4] N. Patwari, J. Ash, S. Kyperountas, A. Hero, R. Moses, and N. Correal, "Locating the nodes: cooperative localization in wireless sensor networks," *Signal Processing Magazine, IEEE*, vol. 22, no. 4, pp. 54–69, 2005.

[5] J. Bosse, A. Ferreol, and P. Larzabal, "A glance on geographical positioning," in *Computational Advances in Multi-Sensor Adaptive Processing (CAMSAP), 2011 4th IEEE International Workshop on*, 2011, pp. 45–48.

[6] P. Meissner and K. Witrisal, "Multipath-assisted single-anchor indoor localization in an office environment," in *Systems, Signals and Image Processing (IWSSIP), 2012 19th International Conference on*, 2012, pp. 22–25.

[7] S. Van de Velde, H. Wymeersch, P. Meissner, K. Witrisal, and H. Steendam, "Cooperative multipath-aided indoor localization," in *Wireless Communications and Networking Conference (WCNC), 2012 IEEE*, 2012, pp. 3107–3111.

[8] S. Van de Velde and H. Steendam, "Cupid algorithm for cooperative indoor multipath-aided localization," in *Indoor Positioning and Indoor Navigation (IPIN), 2012 International Conference on*, 2012, pp. 1–6.

[9] T. Minka, "Divergence measures and message passing," *Microsoft Research, Tech. Rep. MSR-TR-2005-173*, Dec. 2005. [Online]. Available: ftp://ftp.research.microsoft.com/pub/tr/TR-2005-173.pdf

[10] A. Ihler, J. Fisher, R. Moses, and A. Willsky, "Nonparametric belief propagation for self-localization of sensor networks," *Selected Areas in Communications, IEEE Journal on*, vol. 23, no. 4, pp. 809–819, 2005.

[11] S. Rice, "Mathematical analysis of random noise," *Bell System Technical Journal*, vol. 23, pp. 282–332, 1944.

[12] Nist digital library of mathematical functions. [Online]. Available: http://dlmf.nist.gov

[13] J. Hershey and P. Olsen, "Approximating the kullback leibler divergence between gaussian mixture models," in *Acoustics, Speech and Signal Processing, 2007. ICASSP 2007. IEEE International Conference on*, vol. 4, 2007, pp. IV317–IV320.

[14] S. Gezici, Z. Tian, G. Giannakis, H. Kobayashi, A. Molisch, H. Poor, and Z. Sahinoglu, "Localization via ultra-wideband radios: a look at positioning aspects for future sensor networks," *Signal Processing Magazine, IEEE*, vol. 22, no. 4, pp. 70–84, 2005.